A novel miR-99b-5p-*Zbp1* pathway in microglia contributes to the pathogenesis of schizophrenia

Lalit Kaurani[#*1], Md Rezaul Islam*[1], Urs Heilbronner*[2], Dennis M. Krüger[1], Jiayin Zhou[1], Aditi Methi[1], Judith Strauss[3], Ranjit Pradhan[1], Susanne Burkhardt[1], Tonatiuh Pena[1], Lena Erlebach[4], Anika Bühler[4], Monika Budde[2], Fanny Senner[2], Mojtaba Oraki Kohshour[2], Eva C. Schulte[2,5,, 6,7], Max Schmauß[8], Eva Z. Reininghaus[9], Georg Juckel[10], Deborah Kronenberg-Versteeg[4], Ivana Delalle[11], Francesca Odoardi[3], Alexander Flügel[3], Thomas G. Schulze[#2], Peter Falkai[#5], Farahnaz Sananbenesi[#12], Andre Fischer[#1, 13, 14]

* These authors contributed equally to this work

Co-corresponding authors: lalit.kaurani@dzne.de; thomas.schulze@med.uni-muenchen.de; peter.falkai@med.uni-muenchen.de; fsananb@gwdg.de; a.fischer@mail.gwdg.de

[1]Department for Epigenetics and Systems Medicine in Neurodegenerative Diseases, German Center for Neurodegenerative Diseases (DZNE) Goettingen, 37077 Goettingen, Germany

[2]Institute of Psychiatric Phenomics and Genomics (IPPG), University Hospital, LMU Munich, Germany

[3]Institute for Neuroimmunology and Multiple Sclerosis Research, University Medical Center Göttingen, Göttingen, Germany

[4]Department of Cellular Neurology, Hertie Institute for Clinical Brain Research, University of Tübingen, Germany; Germany and German Center for Neurodegenerative Diseases (DZNE) Tübingen, Germany

[5]Department of Psychiatry and Psychotherapy, University Hospital, LMU Munich, Germany

[6]Department of Psychiatry and Psychotherapy, University Hospital Bonn, Medical Faculty, University of Bonn, Bonn, Germany.

[7]Institute of Human Genetics, University Hospital Bonn, Medical Faculty, University of Bonn, Bonn, Germany.

[8]Clinic for Psychiatry, Psychotherapy and Psychosomatics, Augsburg University, Medical Faculty, Bezirkskrankenhaus Augsburg, Augsburg, 86156, Germany

[9]Department of Psychiatry and Psychotherapeutic Medicine, Research Unit for Bipolar Affective Disorder, Medical University of Graz, Graz, 8036, Austria [eva.reininghaus@medunigraz.at]

[10]Department of Psychiatry, Ruhr University Bochum, LWL University Hospital, Bochum, 44791, Germany

[11]Department of Pathology, Lifespan Academic Medical Center, Alpert Medical School of Brown University, Providence, RI 02903, USA

[12]Research Group for Genome Dynamics in Brain Diseases, 37077 Goettingen, Germany.

[13]Department of Psychiatry and Psychotherapy, University Medical Center Goettingen, 37077 Goettingen, Germany

[14]Cluster of Excellence "Multiscale Bioimaging: from Molecular Machines to Networks of Excitable Cells" (MBExC), University of Göttingen, Germany

Abstract

Schizophrenia is a psychiatric disorder that is still not readily treatable. Pharmaceutical advances in the treatment of schizophrenia have mainly focused on the protein coding part of the human genome. However, the vast majority of the human transcriptome consists of non-coding RNAs. MicroRNAs are small non-coding RNAs that control the transcriptome at the systems level. In the present study we analyzed the microRNAome in blood and postmortem brains of controls and schizophrenia patients and found that miR-99b-5p was downregulated in both the prefrontal cortex and blood of patients. At the mechanistic level we show that inhibition of miR-99b-5p leads to schizophrenia-like phenotypes in mice and induced inflammatory processes in microglia linked to synaptic pruning. The miR-99b-5p-mediated inflammatory response in microglia depended on *Z-DNA binding protein 1* (*Zbp1*) which we identified as a novel miR-99b-5p target. Antisense oligos (ASOs) against *Zbp1* ameliorated the pathological phenotypes caused by miR-99b-5p inhibition. In conclusion, we report a novel miR-99b-5p-*Zbp1* pathway in microglia that contributes to the pathogenesis of schizophrenia. Our data suggest that strategies to increase the levels of miR-99b-5p or inhibit *Zbp1* could become a novel therapeutic strategy.

Introduction

Schizophrenia (SZ) is a devastating psychiatric disorder, and the difficulties involved in treating and managing it make it one of the ten most expensive disorders for health care systems worldwide [1] [2]. SZ is believed to evolve on the background of complex genome-environment interactions that alter the cellular homeostasis as well as the structural plasticity of brain cells. Thus, genetic predisposition and environmental risk factors seem to affect processes that eventually contribute to the manifestation of clinical symptoms [3] [4] [5]. Despite the available pharmacological and non-pharmacological treatment options, a significant number of patients do not benefit from these treatments in the long-term, underscoring the need for novel and potentially stratified therapeutic approaches [6]. So far, drug development has focused on the human transcriptome that encodes proteins, but the success of this approach is limited [7]. However, most of the transcriptome consists of non-coding RNAs (ncRNAs) which are recognized as key regulators of cellular functions [8]. Therefore, RNA therapeutics represent an emerging concept that may expand current therapeutic strategies focused on the protein-coding part of our genome [9] [10]. RNA therapies utilize, for example, antisense oligonucleotides (ASOs), siRNA, microRNA (miR) mimics or corresponding anti-miRs to control the expression of genes and proteins implicated in disease onset and progression [11] [9]. Of particular interest are miRs, which are 19-22 nucleotide-long RNA molecules that regulate

protein homeostasis via binding to target mRNAs, leading either to their degradation or reduced translation [12]. miRs have been intensively studied as biomarkers and therapeutic targets in cancer [11] and cardiac diseases [13]. There is also emerging evidence from genetic studies in humans as well as functional data from mouse models that miRs play a role in CNS diseases including SZ [14] [15] [16] [17]. In addition, several studies reported changes in miR expression in blood samples of SZ patients using either qPCR analysis of selected targets or genome-wide approaches. The current findings have been summarized in several review articles [18] [19] [20]. Despite this progress, there are still only few reports on the function of candidate miRs [21]. Nevertheless, analysis of miRs in liquid biopsies is highly valuable because one miR can affect many target genes, and thus changes in miR expression can indicate the presence of multiple pathologies [22] [14] [23]. Moreover, miRs also participate in inter-organ communication [24] [25], suggesting that alterations of miR expression in liquid biopsies may inform about relevant pathological processes in other organs, including the brain. This is important since the analysis of the molecular processes underlying neuropsychiatric diseases in post-mortem human brain tissue is challenging because it might be affected e.g. by peri-mortem events or the timing of post-mortem tissue sampling. Furthermore, the onset of the disease often precedes tissue collection by decades. In contrast, liquid biopsies such as blood samples are easy to collect on the premise that molecular changes in blood mirror changes in the brain. In this context, the analysis of the microRNAome in liquid biopsies could be a suitable approach to identify candidate microRNAs that may play a role in the onset and progression of SZ.

In the present study we performed small RNA sequencing in blood samples of control participants (n = 331) and schizophrenia patients (n = 242) of the PsyCourse Study [26] (http://www.psycourse.de/). By cross-correlating our findings with data from post-mortem human brain tissue, we identified miR-99b-5p as a promising biomarker candidate that is decreased in blood and in the prefrontal cortex of SZ patients, and correlates with disease phenotypes. Furthermore, we found decreased levels of miR-99b-5p in the prefrontal cortex of mice to elicit SZ-like phenotypes and activate pathways linked to innate immunity. In line with these observations, inhibition of miR-99b-5p in microglia increased phagocytosis and reduced the number of synapses. Finally, we were able to demonstrate that this effect is controlled by the miR-99b-5p target gene *Zbp1*, an upstream regulator of innate immunity [27]. Taken together, our data suggest that targeting miR-99b-5p or its target *Zbp1* could provide a novel approach towards the treatment of SZ patients.

Results

miR-99b-5p expression is decreased in SZ patients

105 To identify microRNAs that play a role in the pathogenesis of SZ, we conducted small RNA sequencing
106 of blood samples obtained from 573 participants of the PsyCourse Study (http://www.psycourse.de/).
107 We analyzed 331 healthy controls and 242 SZ patients **(Fig. 1a, Fig. EV1, supplemental table 1)** [26].
108 After data normalization and correction for confounding factors, we performed a weighted gene co-
109 expression network analysis (WGCNA) and detected 8 co-expression modules that significantly
110 differed between groups. Three were significantly decreased **(Fig. 1b)** while 5 were increased **(Fig. 1c)**
111 in SZ patients **(supplemental table 2)**. The turquoise, yellow, blue and red modules displayed the most
112 significant differences among the groups ($P < 0.0001$). We then investigated whether the expression
113 levels of any of these modules correlated with the clinical phenotypes defined by the positive and
114 negative syndrome rating scale (PANSS) and Beck depression inventory (BDI-II), both of which are
115 decreased in SZ patients, and/or the global assessment of functioning (GAF) score, which is increased
116 in these patients **(Fig. EV1)**. Out of the 8 co-expression modules the turquoise, yellow, blue and red
117 modules were significantly correlated to all disease phenotypes. The turquoise module exhibited a
118 significant negative correlation to the PANSS and BDI-II score and a positive correlation with the GAF
119 score **(Fig. 1d)**, which is in line with the decreased expression of this module in SZ. The green, yellow,
120 blue and red modules were positively correlated to the PANSS and BDI-II scores and exhibited a
121 negative correlation with the GAF score, which is in agreement with their increased expression in SZ
122 **(Fig. 1d)**. The pink module was negatively correlated to the PANSS scores and positively correlated to
123 the GAF, which is also in agreement with its decreased expression in SZ patients. However, the pink
124 module was not correlated to the BDI-II score **(Fig. 1d)**. The black and the brown modules were not
125 significantly correlated any of the analyzed phenotypes. Taken together, these data suggest that
126 especially the microRNAs present in turquoise, pink, green, blue, yellow and red modules warrant
127 further analysis. When we subjected the confirmed targets of the microRNAs present within each of
128 these modules to a GO-term analysis, we observed that most modules were linked to inflammatory
129 processes, which is in agreement with a suggested role of neuro-inflammation in the pathogenesis of
130 SZ [28] **(Fig. EV2; Supplemental table 3)**. While WGCNA is a suitable first approach to identify groups
131 of candidate microRNAs, we also performed a differential expression analysis to directly compare the
132 microRNAome in control vs SZ patients. We found 59 microRNA that were significantly increased in SZ
133 patients while 34 microRNAs were decreased **(Fig 1e, Supplemental table 4).**
134 With the aim to further refine the list of candidate microRNAs that may play a role in the pathogenesis
135 of SZ, we performed small RNA sequencing from the prefrontal cortex of SZ patients (n=13) and
136 controls (n=17). We detected 36 microRNAs that were significantly decreased in SZ patients (FDR <
137 0,01, log2FC > 1) and 32 that were significantly upregulated **(Fig. 1f, supplemental table 5)**. Next, we
138 examined whether any of these microRNAs are also found among the differentially expressed

139 microRNAs that were altered in blood samples when compared via differential expression analysis,
140 and within the co-expression modules decreased in SZ patients. Three miRs of the yellow cluster were
141 significantly increased in the brain and in the blood when analyzed via differential expression analysis.
142 In addition, one miR of the blue and one of the green clusters were also increased in brain and blood.
143 These were miR-101-3p, miR-378a-3p, miR-21-5p, miR-192-5p and miR-103a-3p **(supplemental table**
144 **6)**. MiR- 21-3p has been associated with SZ while the other 4 miRs have been studied in the context
145 of other neuropsychiatric or neurodegenerative diseases **(supplemental table 6)**. When analyzing the
146 down-regulated miRs we found four microRNAs, namely miR-500a-3p, miR-501-3p, miR-221-5p and
147 miR-99b-5p, that were detected in the turquoise module and were also decreased in the postmortem
148 brain of SZ patients **(Fig. 1g)**. Of these 4 microRNAs miR-501-3p has been recently linked to
149 schizophrenia [21] **(supplemental table 6)** while miR-99b-5p was the only candidate that was part of
150 a significantly downregulated co-expression module and was significantly downregulated in the brain
151 and blood of SZ patients when analyzed via differential expression analysis**.**
152 In summary, our data reveal a number of interesting candidate miRs such as miR-501-3p and miR-21-
153 5p that have been already linked to SZ in previous studies [29] [21]. Most of the other miRs have been
154 detected in the context of other brain diseases including Alzheimer's disease (AD), Major depression
155 (MD) or Amytrophic lateral sclerosis (ALS) **(supplemental table 6)**. Expect for miR-500a-3p and miR-
156 221-5p, the expression of all other candidate miRs have is significantly correlated to the PANSSs, GAF
157 and BDI-II scores **(Fig. 1h, Fig. EV3)**. While all of these candidate miRs would warrant further functional
158 analysis in the context of SZ, we decided to focus on miR-99b-5p since it has not been linked to any
159 brain disease yet and comparatively little is known about this miR in general.
160
161 ***Decreasing miR-99b-5p leads to SZ-like phenotypes in mice and the upregulation of genes linked to***
162 ***inflammatory processes***
163 The role of miR-99b-5p in the brain has not been intensively studied and thus no data are available in
164 the context of neuropsychiatric diseases such as SZ, making it a novel candidate in need of further
165 evaluation. Before performing mechanistic studies, we decided to employ mice in a model system to
166 test the hypothesis that decreased expression of miR-99b-5p is causatively linked to the development
167 of SZ-like phenotypes. Therefore, we generated lipid nanoparticles (LNPs) containing locked nucleic
168 acid (LNA) representing miR-99b-5p inhibitors (anti-miR99b) and injected these into the prefrontal
169 cortex (PFC) of mice. LNAs representing a scrambled sequence were used as controls (sc-control). MiR-
170 99b-5p levels were significantly decreased in the PFC when measured 5 or 10 days after the injections
171 **(Fig 2a)**. To test schizophrenia-like behaviors in animals, we injected either anti-miR-99b or sc-control
172 to the PFC of mice. Explorative behavior measured in the open field test was similar in all groups **(Fig**

173 **2b)**. However, anti-miR-99b-treated mice spent less time in the center of the open field, which is
174 indicative of increased anxiety **(Fig 2c)**, a phenotype commonly observed in schizophrenia patients
175 [30]. We also analyzed anxiety behavior in the elevated plus maze test. Anti-miR-99b treated mice
176 spent less time in the open arms, which indicates increased anxiety **(Fig 2d)**. Another valid animal
177 model to test schizophrenia-like behavior in rodents is the pre-pulse inhibition of the startle response
178 (PPI) which is used to measure sensory-gating function [31]. PPI is impaired in SZ patients, can easily
179 be assayed in mice and is impaired in mouse models for SZ [32] [33]. We observed that mice injected
180 with anti-miR-99b displayed significantly impaired PPI responses when compared to the sc-control
181 group **(Fig 2e)**. The basic startle response was unaffected **(Fig. 2f)**, suggesting that decreasing the
182 levels of miR-99b-5p in the PFC of mice can lead to SZ-like phenotypes.
183 To gain first insights into the molecular processes controlled by miR-99b-5p in the brain, we injected
184 another group of mice with anti-miR-99b and sc-control oligonucleotides and isolated PFC tissue 5
185 days later for RNA sequencing analysis. Differential expression analysis revealed 147 deregulated
186 genes (adjusted *p*-value < 0.1, log2FC +/- 0.2), of which 113 genes were upregulated and 34 were
187 downregulated **(Fig. 2g; supplemental table 7)**. Gene ontology (GO) analysis revealed that
188 upregulated genes were linked to processes such as innate immunity and interferon signaling **(Fig.**
189 **2h)**. GO analysis of the downregulated genes did not yield any highly significant pathways but detected
190 processes linked to voltage-gated potassium channels **(Fig 2h, supplemental table 8)**. These data
191 suggest that miR-99b-5p in the PFC may regulate mRNAs linked to immune-related processes. To
192 further test this hypothesis, we compared the list of upregulated genes with gene expression data
193 from neurons, astrocytes and microglia as well as genes present within 3 different immune function-
194 related gene expression databases. We observed that the upregulated genes were highly enriched in
195 microglia (P = 4 x 10^{-12}), while no enrichment was observed in astrocytes or neurons. The
196 downregulated genes were significantly enriched in neurons (P = 1.38 x 10^{-12}). In line with this, the
197 upregulated genes were significantly overrepresented in 3 databases for genes linked to immune
198 function, namely the immune, immunome and IRIS databases **(Fig. 2i)**. Together, these data suggest
199 that the levels of miR-99b-5p in the PFC of mice may specifically increase the expression of immune-
200 related genes in microglia. To further test this we administered anti-miR-99b or sc-control to the PFC
201 of mice and subsequently isolated $CD45^{low}/CD11b^{+}$ microglial cells via fluorescence-activated cell
202 sorting (FACS). While microglia cell numbers did not differ between groups**,** miR-99b-5p expression
203 was significantly decreased in microglia isolated from anti-miR-99b-treated mice **(Fig. EV4).** The
204 expression of selected pro-inflammatory genes *Il1ß, Tgfb1* and *Tnfα* that were upregulated in the RNA-
205 seq dataset were also increased in microglia obtained from anti-miR-99b-treated mice, although *Tgfβ1*
206 failed to reach significance (P = 0.08) **(Fig 2j)**.

207 These data suggest that miR-99b-5p controls microglia-mediated immunity in the PFC, which is in
208 agreement with previous studies linking aberrant microglia function and neuroinflammation to the
209 pathogenesis of SZ [34].
210
211 ***miR-99b-5p controls microglia-mediated immune function and affects dendritic spine number***
212 To further explore the role of miR-99b-5p in microglia, we cultured primary microglia from the cortex
213 of mice and treated these cells with anti-miR-99b or sc-control LNAs followed by RNA sequencing **(Fig**
214 **3a)**. Differential expression analysis revealed 139 deregulated genes, of which 104 were up- and 35
215 were downregulated **(Fig 3b, supplemental table 9)**. GO-term and KEGG-pathway analysis revealed
216 that the upregulated genes were linked to immune activation and phagocytosis **(Fig 3c; supplemental**
217 **table 10)**. In agreement with the *in vivo* data, we observed an increased expression of *Il1ß, Tgfb1, and*
218 *Tnfα*, which could be confirmed via qPCR **(Fig 3d; see also Fig EV4c)**. Next, we investigated
219 phagocytosis, a key function of microglia that is altered during neuroinflammation [35]. In a first
220 approach we employed immortalized microglia (IMG) cells. Similar to the treatment with the
221 lipopolysaccharide (LPS) commonly used to induce microglia activation, inhibition of miR-99b-5p
222 caused an upregulation of proinflammatory cytokines and increased phagocytosis as measured via the
223 uptake of fluorescent latex beads **(Fig. EV5)**. Encouraged by these data we performed similar
224 experiments in primary microglia isolated from the mouse PFC. In line with the data obtained in IMG
225 cells, treatment of primary microglia with anti-miR-99b LNAs significantly increased phagocytosis **(Fig**
226 **3e)**.
227 Aberrant microglia activity can have detrimental effects on neuronal plasticity [36]. To test whether
228 the reduced expression of miR-99b-5p in microglia could affect neuronal plasticity, we performed a
229 co-culturing experiment. Primary microglia were first treated with sc-control or anti-miR-99b LNAs for
230 48 h before being harvested and transferred to cortical neuronal cultures **(Fig 3f)**. RNA was isolated
231 from these co-cultures after 48 h and subjected to RNA-seq. Differential expression analysis revealed
232 366 deregulated genes (155 upregulated and 211 downregulated genes, adjusted p value < 0.05,
233 log2FC +/- 0.1); **Fig. 3g, supplemental table 11**). GO term analysis of the upregulated genes revealed
234 neuroinflammatory processes, neuron death, neuron apoptotic processes as well as synaptic pruning
235 **(Fig 3h, supplemental table 12_UP)**, while downregulated genes were associated with processes
236 indicating loss of synaptic function such as regulation of axon extension or synapse organization **(Fig**
237 **3h, supplemental table 12_DOWN)**.
238 These data are in agreement with our previous findings suggesting that loss of miR-99b-5p increases
239 inflammatory processes in microglia. More importantly, the data suggest that microglia lacking miR-
240 99b-5p may have detrimental effects on synaptic function when co-cultured with cortical neurons. It

241 is particularly interesting that synaptic pruning is detected as a major process increased in the co-
242 cultures, since synaptic pruning has been linked to SZ [36]. In line with this, key factors of the
243 complement system known to drive pathological synaptic pruning were increased in primary microglia
244 treated with anti-miR-99b, as well as in the corresponding co-cultures and also in the postmortem
245 human prefrontal cortex of schizophrenia patients **(Fig EV6)**. When we analyzed the number of
246 dendritic spines, we observed that spine density was significantly reduced in neurons co-cultured with
247 microglia that had received anti-miR-99b, when compared to cultures treated with corresponding
248 control microglia **(Fig 3 i)**.
249
250 ***miR99b-5p control neuroinflammation via the regulation of Zbp1***
251 The three RNAseq datasets obtained from the PFC of mice, primary microglia and the co-cultures
252 consistently show that knockdown of miR-99b-5p increases the expression of genes linked to
253 inflammatory processes. Many of the gene expression changes likely represent secondary effects. To
254 better understand the mechanisms by which miR-99b-5p controls neuroinflammation, we aimed to
255 identify direct targets of miR-99b-5p (**supplemental table 13**). When we analyzed the RNA-seq data
256 obtained from the PFC (see Fig 2), we identified 13 out of 113 genes as potential mRNA targets of
257 miR99b-5p **(Fig 4A)**. GO term analysis was performed for the 13 genes and revealed that they are
258 linked to inflammatory processes including type I interferon signaling **(Fig. EV7, supplemental table**
259 **14)**, linked to schizophrenia [37] [38]. Seven of these genes were also upregulated in primary microglia
260 treated with anti-miR-99b, and among them were key regulators of inflammatory processes such as
261 *Stat1* which was found to be hyperactive in blood samples of SZ patients [39]. A gene that specifically
262 caught our attention was *Zbp1* because the corresponding protein - also known as the DNA-dependent
263 activator of interferon regulatory factors (*Dai*) - is a key regulator of pro-inflammatory processes that
264 result in the activation of inflammatory caspases and the induction of *Il1ß* [27]. Thus, *Zbp1*
265 represented a rather upstream factor in the inflammatory cascade. On this basis, we speculated that
266 the regulation of *Zbp1* could be a key mechanism by which miR-99b-5p regulates inflammatory
267 processes and may contribute to the pathogenesis of SZ when it is increased.
268 First, we performed a luciferase assay to directly test the regulation of *Zbp1* by miR-99b-5p. We used
269 the renilla dual luciferase reporter vector harboring the *Zbp1*-3'UTR. Co-transfection of this vector
270 with miR-99b-5p LNAs significantly reduced the luciferase activity **(Fig 4b)**, but this was not the case
271 when scramble control LNAs were used **(Fig 4b)**. Moreover, we observed that ZBP1 protein levels were
272 significantly increased in primary microglia treated with anti-miR-99b **(Fig 4c)**. These data show that
273 miR-99b-5p can directly regulate *Zbp1* levels.
274

275 On this basis we decided to investigate whether the inflammatory phenotypes induced in response to
276 decreased miR-99b-5p levels depend on *Zbp1*. So far, we have found that decreased levels of miR-
277 99b-5p lead to enhanced phagocytosis and increased expression of pro-inflammatory cytokines such
278 as *Il1ß* which has been associated with *ZBP1* activity [40]. Another important step in ZBP1-mediated
279 orchestration of inflammation is the activation of pro-inflammatory caspases [41] [42], and therefore
280 we examined whether reduced miR-99b-5p levels would also affect the activity of pro-inflammatory
281 caspases. Indeed, when primary microglia were treated with anti-miR-99b, caspase activity was
282 significantly increased when compared to that in cells treated with sc-control LNAs **(Fig. 4d)**. Similar
283 findings were obtained when protein lysates isolated from the PFC of mice injected with either anti-
284 miR-99b or sc-control LNAs were analyzed for caspase activity **(Fig. 4e)**.
285 To test whether the miR-99b-5p-mediated increase in caspase activity, *IL-1ß* expression and
286 phagocytosis depends on *Zbp1*, we treated primary microglia with either anti-miR-99b alone or in
287 combination with an anti-sense oligonucleotide (ASO) targeting *Zbp1* (*Zbp1*-ASO). In agreement with
288 our previous observation, anti-miR-99b treatment increased caspase activity. This effect was
289 ameliorated in microglia treated with anti-miR-99b and *Zbp1*-ASO **(Fig 4f)**. Similar observations were
290 made when we analyzed *IL1ß* expression **(Fig. 4g)** and phagocytosis **(Fig 4h)**. These data suggest that
291 ZBP-1 plays an important role in mediating the neuroinflammatory processes downstream of miR-
292 99b-5p.
293 We performed parallel experiments in human iPSC-derived microglia. Similar to the mouse data,
294 administration of anti-miR-99b increased caspase activity **(Fig 4i)**, IL-1ß expression **(Fig 4j)** and
295 phagocytosis **(Fig 4k)** when compared to human iPSC-derived microglia treated with sc-control LNAs.
296 These effects were attenuated when anti-miR-99 LNAs were co-administered with *Zbp1*-ASOs **(Fig 4i-**
297 **k)**. These data suggest that in human microglia, miR-99b-5p also controls neuroinflammatory
298 processes via the regulation of *Zbp-1* expression. In line with this interpretation, IL1ß and Zbp1 mRNA
299 levels were increased in postmortem human brain samples from SZ patients and controls **(Fig. S8a)**.
300 To determine whether knockdown of *Zbp1* would also mitigate the effect of anti-miR-99b treatment
301 on SZ-like behavior in mice, we injected either anti-miR-99b alone or in combination with *Zbp1*-ASOs
302 into the PFC of mice before subjecting the animals to behavior testing. Mice injected with sc-control
303 LNAs served as controls. The corresponding data revealed that *Zbp1* knockdown rescues anti-miR-99b-
304 mediated impairment of PPI **(Fig. S8)**.
305 Our findings suggest that reduced miR-99b-5p levels in microglia contribute to the pathogenesis of
306 schizophrenia via the regulation of *Zbp1*-controlled neuroinflammation. Therefore, miR-99b-5p may
307 constitute a novel biomarker for SZ, while targeting miR-99b-5p and/or ZBP1 might represent an
308 effective SZ treatment

309
310 **Discussion**

311 In this study we combined the analysis of blood samples and postmortem brain tissue to identify
312 miRs involved in the pathogenesis of SZ. Using WGCNA as well as differential expression analysis in
313 blood samples, we identified several miRs that differed between patients and controls and were
314 significantly correlated with SZ phenotypes. GO term analysis of the confirmed target genes of these
315 miRs hinted at a number of molecular processes of which pathways linked to immune function were
316 overrepresented. Such a GO term analysis based on miR target genes is, of course, not ultimately
317 conclusive but our observation is in agreement with previous studies showing that neuroinflammation
318 plays a role in the pathogenesis of SZ [43] [44]. To further refine the identification of miRs linked to SZ
319 we also performed a differential expression analysis of the small RNA seq data obtained from blood
320 as well as from postmortem brain tissue of SZ patients and controls. We eventually identified five
321 candidate miRs, miR-101-3p, miR-378a-3p, miR-21-5p, miR-192-5p and miR-103a-3p, that were
322 increased in the blood and brain of SZ patients. All of these miRs have been implicated brain and non-
323 brain diseases. For example, knock-down of miR-101-3p in the hippocampus impairs learning in mice
324 [45] while increased circulating levels of miR-101-3p have been observed in patients suffering from
325 autism [46], attention-deficit hyperactivity disorder [47] but also diabetes [48] [49] or cancer [50].
326 MiR-378a-3p has been associated with cerebral ischemia [51] is increased in blood samples of Down
327 syndrome patients [52] and was reported to be part of a blood-miR signature that can distinguish
328 Alzheimer's disease patients from control [53]. miR-21-5p was found to be increased in blood samples
329 of SZ patients [29], while antipsychotic treatment is correlated with decreased miR-21-3p expression
330 [54]. Moreover, miR-21-3p was altered in blood samples of patients suffering from bipolar disease
331 [55]. However, altered miR-21-3p has also been observed in various other diseases and is for example
332 increased in patients with lung cancer [56]. Several studies have linked miR-192-5p to cognitive
333 function and depression. For example, miR-192-5p was decreased in the blood AD patients upon
334 aerobic exercise [57] and was altered in the brains of patients suffering from major depressive
335 disorder [58], while increasing the levels of miR-192-5p in a mouse model for depression ameliorated
336 cognitive impairments [59]. Finally, altered blood levels of miR-103-3p have been linked to childhood
337 traumatization and depression [60] as well as Autism [61].

338 Four miRs, miR-500a-3p, miR-501-3p, miR-221-5p and miR-99b-5p, that all originated from the
339 ME_Turquoise co-expression module which was downregulated in SZ patients and significantly
340 correlated to SZ phenotypes, were also decreased in the postmortem brains of SZ patients . A recent
341 study identified miR-501-3p as a schizophrenia-associated miR as it was found to be decreased in
342 blood samples of monozygotic twins discordant for SZ [21]. The authors went on to show that loss of
343 miR-501-3p in mice leads to SZ-like phenotypes, a finding that was linked to miR-501-3p-mediated

344 regulation of *metabotropic glutamate receptor 5* expression in the cortex. These data are in
345 agreement with our observation that miR-501-3p was decreased in SZ patients of the PsyCourse study
346 as well as in the postmortem brains of SZ patients. As to the other 3 miRs, there are thus far no data
347 on the role of miR-500a-3p in the CNS, and while miR-221-5p has recently been linked to the regulation
348 of synaptic processes [62], there are still also no data on the role of miR-221-5p in SZ. As regards to
349 miR-99b-5p, no functional data are available on its role in the CNS, and no report has as yet implicated
350 this miR in the pathogenesis of SZ.

351 In summary, we have discovered miRs that have already been linked to the pathogenesis of SZ or
352 other brain diseases, as well as miRs that have not been extensively studied so far. These data
353 suggests that our approach may provide a viable means to detect novel SZ-associated miRs.

354 To test this hypothesis, we decided to investigate miR-99b-5p that was part of the ME_Turquoise
355 co-expression module but was also decreased in the postmortem brain of SZ patients as well as in the
356 blood of SZ patients, when the data was analyzed via differential expression. Moreover, essentially
357 nothing was known about the role of miR-99b-5p in the adult brain. Inhibiting miR-99b-5p in the
358 prefrontal cortex of mice led to impaired PPI and increased anxiety. PPI is impaired in SZ patients and
359 in mouse models for SZ [32] [33]. Furthermore, increased anxiety is a phenotype often observed in SZ
360 patients [30], suggesting that reduced miR-99b-5p levels are indeed linked to the development of SZ-
361 like phenotypes. Nevertheless, these data cannot establish a clearly causal link between reduced miR-
362 99b-5p expression and the pathogenesis of SZ in humans, since no animal model can fully recapitulate
363 the complex processes in human patients due to functional and structural differences in cortical
364 anatomy [63] [64].

365 However, that miR-99b-5p is involved in the pathogenesis in SZ is further underscored by the
366 results of our molecular analysis. RNA-seq analysis of the prefrontal cortex of mice revealed that
367 inhibition of miR-99b-5p mainly led to an increased expression of genes, which is in agreement with
368 the established action of miRs in controlling mRNA levels. Furthermore, the upregulated genes were
369 almost exclusively related to immunity pathways in microglia, a process which has been linked to the
370 pathogenesis of SZ by various means. For example, altered microglia have been observed in
371 postmortem brain samples of SZ patients [65]. In addition, epidemiological data demonstrated a
372 correlation between immune diseases and SZ [66], while several neuroimaging studies reported an
373 increase in activated microglia in the brains of SZ patients [67] [68]. Finally, studies in animal models
374 have implicated aberrant microglia activation with the onset of SZ-like phenotypes [69] [70]. While
375 miR-99b-5p has not been studied in microglia so far, these data are in line with previous reports
376 demonstrating a role of the miR-99b in the modulation of inflammatory responses. For example, miR-
377 99b levels are decreased in tumor-associated macrophages and re-expression of miR-99b attenuates

378 tumor growth [71]. Furthermore, inhibition of miR-99b in dendritic cells significantly elevated the
379 levels of proinflammatory cytokines including *Il1ß* and *Tnfα* [72]. These findings are in agreement with
380 our data showing that inhibition of miR-99b-5p in the prefrontal cortex of mice increased the
381 expression of pro-inflammatory cytokines including *Il1ß* and *Tnfα* in microglia that we had isolated
382 from the brains of these mice via FACS. A strong upregulation of genes linked to inflammatory
383 processes, including the upregulation of *Il1ß* and *Tnfα,* was also observed when miR-99b-5p was
384 inhibited in IMG cells or primary microglia. This is interesting since increased *Ill1 ß* and *Tnfα* levels
385 have been repeatedly reported in SZ patients [73] and may offer novel therapeutic avenues. For
386 example, inhibition of TNF*α* was recently shown to ameliorate disease phenotypes in different mouse
387 models of SZ [70].
388 Aberrant microglia activation can affect neuronal function via synaptic pruning, a process that is
389 based on the phagocytic activity of microglia [74]. We observed that inhibition of miR-99b-5p in IMG
390 cells and in primary microglia increased their phagocytic activity. Moreover, cortical neurons co-
391 cultured with microglia that were treated with anti-miR-99b oligonucleotides displayed differentially
392 expressed genes, of which the downregulated genes were linked to GO terms such as synapse
393 assembly, regulation of synaptic plasticity or dendritic spine organization. As for the upregulated
394 genes, the most significant GO term was synapse pruning. Since our data also revealed that neurons
395 co-cultured with anti-miR-99b-treated microglia indeed displayed a reduced number of dendritic
396 spines, our findings suggest a scenario in which reduced levels of miR-99b-5p lead to an upregulation
397 of proinflammatory processes in microglia, which eventually impacts on synaptic structure. This
398 interpretation is in agreement with previous reports suggesting that aberrant microglia activation
399 leads to pathological synaptic pruning, which in turn leads to plasticity defects which could drive the
400 pathogenesis of SZ [36] [75]. Notably, the increased expression of several complement factors in
401 microglia have been implicated in this process [76]. In line with these data, we observed increased
402 expression of key complement factors in primary microglia and in corresponding microglia/neuron co-
403 cultures in which miR-99b-5p was inhibited, as well as in postmortem brain samples from SZ patients.
404 In summary, these findings provide a plausible mechanism on how reduced levels of miR-99b-5p can
405 contribute to the pathogenesis of SZ, namely the induction of a pro-inflammatory response associated
406 with synaptic pruning. Nevertheless, we cannot exclude that additional mechanisms within microglia
407 or other neural cells play a role.
408 MiRs mediate their biological action by controlling the expression of specific target mRNAs. Our data
409 showed that within microglia, miR-99b-5p controls the expression of the *Zbp1* gene that plays an
410 important role in the innate immune response [27]. ZBP1 acts as sensor for Z-DNA/Z-RNA and controls
411 inflammatory pathways such as type I interferon-signaling and other pathways, eventually leading to

412 the upregulation of various pro-inflammatory cytokines including e.g. the induction of *IL1ß* [77] [78]
413 [40].
414 These data suggest that reduced levels of miR-99b-5p in microglia contribute to SZ-like
415 phenotypes because the tight control of *Zbp1* levels is lost. In line with this interpretation, we
416 demonstrated that the administration of *Zbp1*-ASO rescues the effects of anti-miR-99b treatment on
417 SZ-like phenotypes in mice as well as in the corresponding cellular alterations observed in primary
418 microglia from mice as well as in microglia derived from human iPSCs. Interestingly, the cellular
419 processes we find to be affected by altered miR-99b-5p and *Zbp1* levels have also been implicated in
420 other brain diseases. Thus, it will be important to investigate the role of miR-99b-5p and *Zbp1* in other
421 neuropsychiatric diseases. Moreover, aberrant microglia activation and synaptic pruning is observed
422 in neurodegenerative diseases such as Alzheimer's disease [79], and ZBP1 also controls the NRLP3
423 inflammasome [78], a key regulator of neuroinflammatory phenotypes in Alzheimer's disease [80]. In
424 this context it is interesting to note that one study found decreased miR-99b-5p levels in plasma
425 samples obtained in a mouse model of Alzheimer's disease when measured at 6 and 9 months of age,
426 while increased levels were reported in older mice [81]. These data might underscore the need for
427 further study as to the role of *miR-99b-5p* and *Zbp1* in microglia obtained from wild type mice as well
428 as mouse models for neuropsychiatric or neurodegenerative diseases at different ages. Indeed, it is
429 well established that microglia undergo age-dependent functional changes and even differ between
430 brain regions [82] [83].
431 There are other questions we could not address within the scope of this manuscript. It will for
432 example be interesting to investigate the other candidate miRs we found in addition to miR-99b-5p.
433 Similarly, it will be important to study the potential miR-99b-5p targets we found in addition to *Zbp-1*
434 in the context of SZ. Another question relates to the mechanisms that underlie the downregulation of
435 miR-99b-5p in SZ patients. In future projects it will be interesting to test for example whether miR-
436 99b-5p is altered in SZ mouse models that are based on either genetic or environmental risk factors
437 such as early life stress. In addition, it will be important to identify the source of elevated miR-99b-5p
438 levels in blood samples of SZ patients. It is known that miRs can be transported from the brain to the
439 periphery within exosomes [84] [25], and recent studies reported the isolation of microglia-derived
440 exosomes from human blood [85]. While this approach is not undisputed, it will be interesting to apply
441 such methods to the PsyCourse Study, which is, however, beyond the scope of the current work.
442 Although our findings that miR-99b-5p is decreased in the brain and the blood of SZ patients support
443 the idea that the changes in blood may reflect corresponding changes in the brain, we cannot
444 conclusively answer this question at present. Rather, we suggest that the analysis of miR-99b-5p levels

445 in blood may eventually help stratify patients for treatment, including novel approaches based on RNA
446 therapeutics towards miR-99b-5p or *Zbp1*.
447 In conclusion, in the present study we identify a miR-99b-5p-*Zbp1* pathway in microglia as a
448 novel mechanism that likely contributes to the pathogenesis of schizophrenia. Our data also suggest
449 that strategies to increase the levels of miR-99b-5p or inhibit *Zbp1*, for example via ASOs, could serve
450 as novel therapeutic strategies for treating SZ patients.
451
452 **Material and Methods**
453 *Human subjects:*
454 All experiments involving human data were approved by the relevant Ethics committees (see Budde
455 et al.). Informed written consent was obtained for all subjects. Blood samples (PAXgene Blood RNA
456 Tubes; PreAnalytix, Qiagen) and behavioral data (supplemental table 1) of control and schizophrenia
457 patients were obtained from participants of the PsyCourse Study [26]. Psychiatric diagnoses were
458 confirmed using the Diagnosis and Statistical Manual of Mental Disorders Fourth Edition (DSM-IV)
459 criteria. Control subjects were screened for psychiatric disorders using parts of the structured clinical
460 interviews for mental disorders across the lifespan (MINI-DIPS). All subjects were assessed for
461 psychiatric symptoms through a battery of standard tests including the Positive and Negative
462 Syndrome Scale (PANSS), the Global Assessment of Functioning Scale (GAF), and the Beck depression
463 inventory (BDI-II).
464
465 *Post-mortem human brain samples:*
466 Postmortem tissue samples (prefrontal cortex A9&24) from controls (n = 17; 5 females & 12 males;
467 age = 62.3 ± 18.9 years, PMD = 19.7 ± 6.7 h) and schizophrenia patients (n = 13; 5 females & 8 males;
468 age 57.7 ± 16.8 years, PMD = 21 ± 6.4 h) were obtained with ethical approval and upon informed
469 consent from the Harvard Brain Tissue Resource Center (Boston, USA). RNA was isolated using Trizol
470 as described in the manufacturer protocol using the Directzol RNA isolation kit (Zymo Research,
471 Germany). RNA concentration was determined by UV measurement. RNA integrity for library
472 preparation was assessed using an RNA 6000 NanoChip in a 2100 Bioanalyzer (Agilent Technologies).
473
474 *High throughput small RNAome sequencing:*
475 Small RNAome libraries were prepared with total RNA according to the manufacturer's protocol with
476 NEBNext® small RNA library preparation kit. All human subject small RNAome libraries were prepared
477 with 150 ng of total RNA. Briefly, total RNA was used as starting material, and the first strand of cDNA
478 was generated, followed by PCR amplification. Libraries were pooled and PAGE was run for size

479 selection. For small RNAome, ~150 bp band was cut and used for library purification and
480 quantification. A final library concentration of 2 nM was applied for sequencing. The Illumina HiSeq
481 2000 platform was used for sequencing and was performed using a 50-bp single read setup. Illumina's
482 conversion software bcl2fastq (v2.20.2) was used for adapter trimming and converting the base calls
483 in the per-cycle BCL files to the per-read FASTQ format from raw images. Demultiplexing was carried
484 out using Illumina CASAVA 1.8. Sequencing adapters were removed using cutadapt-1.8.1. Sequence
485 data quality was evaluated using FastQC (http://www.bioinformatics.babraham.
486 ac.uk/projects/fastqc/). Sequencing quality was determined by the total number of reads, the
487 percentage of GC content, the N content per base, sequence length distribution, duplication levels,
488 overrepresented sequences and Kmer content.
489
490 *Da*ta processing, QC, and *Differential expression (DE) analysis:*
491 Sequencing data was processed using a customized in-house software pipeline. Quality control of raw
492 sequencing data was performed by using FastQC (v0.11.5). The quality of miRNAs reads was evaluated
493 by mirtrace (v1.0.1). Reads counts were generated using TEsmall (v0.4.0) which uses bowtie (v1.1.2)
494 for mapping. Reads were aligned to the Homo_sapiens GRCh38.p10 genome assembly (hg38). The
495 miRNA reads were annotated using miRBase. Read counts were normalized with the DESeq2 (v1.26.0)
496 package. Unwanted variance such as batch effects, library preparation effects, or technical variance
497 was removed using RUVSeq for all data (v1.20.0; k = 1 was used for factors of unwanted variation).
498 DeSeq2 was utilized for differential expression analysis and adjustment of confounding factors. In the
499 DESeq2 model, the PsyCourse data were corrected for sex, age and medication in DeSeq2. Volcano
500 plots were plotted with the R package EnhancedVolcano (v1.4.0).
501
502 *WGCNA analysis:*
503 microRNAome co-expression module analysis was carried out using the weighted gene co-expression
504 network analysis (WGCNA) package (version 1.61) in R [86]. We first regressed out age, gender, and
505 other latent factors from the sequencing data, and after that, normalized counts were log (base 2)
506 transformed. Next, the transformed data were used to calculate pairwise Pearson's correlations
507 between microRNAs and define a co-expression similarity matrix, which was further transformed into
508 an adjacency matrix. Next, a soft thresholding power of 8 was chosen based on approximate scale-
509 free topology and used to calculate pairwise topological overlap between microRNAs in order to
510 construct a signed microRNA network. Modules of co-expressed microRNAs with a minimum module
511 size of 10 were later identified using cutreeDynamic function with the following parameters: method
512 = "hybrid", deepSplit =4, pamRespectsDendro =F, pamStage = T. Closely related modules were merged

513 using a dissimilarity correlation threshold of 0.25. Different modules were summarized as a network
514 of modular eigengenes (MEs), which were then correlated with the different psychiatric symptoms
515 and functionality variables (e.g., PANSS, GAF etc). The module membership (MM) of microRNAs was
516 defined as the correlation of microRNA expression profile with MEs, and a correlation coefficient
517 cutoff of 0.5 was set to select the module specific microRNAs. The Pearson correlation of MEs and
518 psychiatric symptoms and functionality variable was plotted as a heat map.
519
520 *Enriched gene ontology and pathways analysis:*
521 To construct the Gene Regulatory network (GRN) for miRNA-target genes we retrieved validated
522 microRNA targets from miRTarBase (v 7.0) (http://mirtarbase.mbc.nctu.edu.tw/). microRNA target
523 genes were further filtered based on the expression in the brain. Brain-enriched expression was
524 examined using the Genotype-Tissue Expression (GTEx) database. (GTEx Consortium). To identify the
525 biological processes and their pathways in the miRNA-target genes, the ClueGO v2.2.5 plugin of
526 Cytoscape 3.2.1 was used [87]. In the ClueGo plugin [88] a two-sided hypergeometric test was used to
527 calculate the importance of each term and the Benjamini-Hochberg procedure was applied for the P
528 value correction. KEGG (https://www.genome.jp/kegg/) and Reactome (https://reactome.org/)
529 databases were used for the pathway analysis. To construct GRN for significantly deregulated mRNAs,
530 the ClueGO v2.2.5 plugin of Cytoscape 3.2.1 was used. Biological processes (BP) and pathways with
531 adjusted p value < 0.05 were selected for further analysis. For further analysis, cellular metabolism
532 and cancer-related biological processes were omitted. Key BPs with low levels of GOLevel (because
533 terms at lower levels are more specific and terms higher up are more general) were further considered
534 for data presentation and interpretation.
535
536 *microRNA and mRNAs lipid nanoparticles preparation:*
537 miR99b-5p inhibitor sequences were used to decrease the expression of miR99b-5p. To decrease the
538 expression of mRNAs, anti-sense oligos (ASO) were employed. ASOs, inhibitor and negative control
539 sequences were purchased from Qiagen. MicroRNA inhibitor, or ASOs lipid nanoparticle (LNP)
540 formulation, was achieved using a proprietary mixture of lipids containing an ionizable cationic lipid,
541 supplied as Neuro9™ siRNA Spark™ Kit (5 nmol). The miRNA inhibitor or ASOs were encapsulated using
542 a microfluidic system for controlled mixing conditions on the NanoAssemblr™ Spark™ system
543 (Precision Nanosystems, Canada). The experiments were performed as described in the
544 manufacturer's protocol. Briefly, 5 nmol lyophilized microRNA inhibitor or ASOs were dissolved in
545 formulation buffer 1 (FB1) to a final concentration of 2 nmol. This solution was further diluted to a
546 final concentration of 930 ug/mL. Formulation buffer 2 (FB 2), microRNA inhibitor/ASOs in FB1, and

547 lipid nanoparticles were added to the cartridge and encapsulated using the NanoAssembler Spark
548 system.
549
550 *Animals*
551 C57BL/6J mice were purchased from Janvier and housed in an animal facility with a 12-h light–dark
552 cycle at constant temperature (23 °C) with *ad libitum* access to food and water. Animal experiments
553 complied with relevant ethical regulations and were performed as approved by the local ethics
554 committee. All experiments were performed with 3 months old male mice. Pre-frontal cortex (PFC)
555 region was dissected on day five after stereotaxic surgery for RNA-seq-based experiments.
556
557 *Stereotaxic surgery:*
558 For intracerebral stereotaxic injections of LNPs in the PFC, 3-month-old mice were anesthetized with
559 Rompun 5mg/kg and Ketavet 100mg/kg. After application of local anesthesia to the skull, two small
560 holes were drilled into the skull. Mice then received a bilateral injection of LNPs of microRNA
561 inhibitor/negative control or ASOs (dose: 0.15 ug/mL for microRNA inhibitor/negative control; dose:
562 0.3 ug/mL for ASO+ microRNA inhibitor mix). LNPs were injected with a rate of 0.3 µl/min per side.
563 Only 0.9 ul of LNPs were injected per hemisphere (0,5 µl/min). After surgery, all mice were monitored
564 until full recovery from the anesthesia and housed under standardized conditions.
565
566 *Behavioral phenotyping:*
567 The open field test was performed to evaluate locomotory and exploratory functions. Mice were
568 placed individually in the center of an open arena (of 1 m length, 1 m width, and side walls 20 cm
569 high). Locomotory activity was recorded for 5 min using the VideoMot2 tracking system (TSE Systems).
570 The elevated plus maze test was used to evaluate basal anxiety. Mice were placed individually in the
571 center of a plastic box consisting of two open and two walled closed arms (10 × 40 cm each, walls 40
572 cm high). Their behavior was recorded for 5 min using the VideoMot2 system. Time spent in open
573 versus closed arms was measured to assay basal anxiety phenotype. Prepulse inhibition (PPI) was
574 performed to test the acoustical startle response (ASR). ASR was completed in an enclosed sound-
575 attenuated startle box from TSA Systems. In brief, mice were placed individually inside a cage attached
576 with a piezoelectric transducer platform in a sound-attenuated startle cabinet. These sensory
577 transducers converted the movement of the platform induced by a startle response into a voltage
578 signal. Acoustic stimuli were executed through speakers inside the box. The mice were given 3 min to
579 habituate at 65 dB background noise and their activity was recorded for 2 min as baseline. After the
580 baseline activity recording, the mice were tested to six pulse-alone trials, at 120-dB startle stimuli

581 intensity for a duration of 40 ms. PPI of startle activity was measured by conducting trials for pre-pulse
582 at 120 dB for 40 ms or preceding non-startling prepulses of 70, 75, 80, 85, 90 dB.
583
584 *RNA isolation:*
585 Humans: PAXgene Blood RNA Tubes (PreAnalytix/Qiagen) were stored at -80°C. For RNA isolation, the
586 tubes were thawed and incubated at room temperature overnight. RNA was extracted according to
587 the manufacturer's protocol using PAXgene Blood RNA Kits (Qiagen). RNA concentrations were
588 measured by UV measurement. RNA integrity for library preparation was determined by analyzing
589 them on an RNA 6000 NanoChip using a 2100 Bioanalyzer (Agilent Technologies).
590 Mice: The mice were sacrificed by cervical dislocation on day five after stereotaxic surgery. Unilateral
591 PFC region was collected and immediately frozen in liquid nitrogen and later stored at -80°C until RNA
592 isolation. Total RNA was isolated using the trizol method as described by the manufacturer's protocol
593 using the Directzol RNA isolation kit (Zymo Research, Germany). The RNA concentration was
594 determined by UV measurement. RNA integrity for library preparation was assessed using a
595 Bioanalyzer (Agilent Technologies).
596
597 *RNA sequencing:*
598 Total RNA was used for the library preparation using the TrueSeq RNA library prep kit v2 (Illumina,
599 USA) according to the manufacturer's protocol. 500 ng RNA was used as starting material. The quality
600 of the libraries was assessed using the Bioanalyzer (Agilent Technologies). Library concentration was
601 measured by Qubit™ dsDNA HS Assay Kit (Thermo Fisher Scientific, USA). Multiplexed libraries were
602 directly loaded onto a Hiseq2000 (Ilumina) with 50 bp single read setup.
603 The sequencing data were processed using a customized in-house software pipeline. Illumina's
604 conversion software bcl2fastq (v2.20.2) was employed for adapter trimming and converting the base
605 calls in the per-cycle BCL files to the per-read FASTQ format from raw images. Quality control of raw
606 sequencing data was carried out using FastQC (v0.11.5)(http://www.bioinformatics.babraham.
607 ac.uk/projects/fastqc/). Reads were aligned using the STAR aligner (v2.5.2b) and read counts were
608 generated using featureCounts (v1.5.1). The mouse genome version mm10 was utilized.
609
610 *Publicly available datasets:*
611 Various publicly available datasets were used in this study to explore cell type-specific expression of
612 differentially expressed genes. Published single cell data [89] were utilized to explore neuron-,
613 astrocyte-, and microglia-specific expression of genes. Immunome-related genes were retrieved from

614 the Immunome database. The Immune Response In Silico (IRIS) dataset was used to explore immunity-
615 related genes [90] [91]
616
617 *Primary microglia cultures:*
618 Primary mouse microglia cell cultures were prepared as previously described for wild-type pups [92].
619 In brief, newborn mice (P1 pups) were used to prepare mixed glia cultures. Cells were grown in DMEM
620 (Thermo Fisher Scientific) with 10% FBS, 20% L929 conditioned medium and 100 U ml–1 penicillin–
621 streptomycin (Thermo Fisher Scientific). Microglia were collected 10-12 days after cultivation by shake
622 off, counted and plated in DMEM supplemented with 10% FBS, 20% L929 conditioned medium and
623 100 U ml–1 penicillin–streptomycin. The microglia were shaken off up to two times.
624
625 *Ex-vivo isolation of microglia:*
626 PFC regions were dissected, mechanically dissociated and digested for 15 minutes with liberase (0.4
627 U/mL; Roche) and DNAse I (120 U/mL; Roche) at 37°C. Subsequently, the cell suspension was passed
628 through a 70 µm cell strainer. Myelin debris was eliminated by the Percoll density gradient. Single cell
629 suspension was labeled by using anti-mouse CD45 BV 421 (Clone 30-F11, Biolegend) and CD11b FITC
630 (Clone M1/70, Biolegend). Antibody-labeled $CD45^{low}$ $CD11b^{+}$ microglial cells were sorted using a
631 FACSAria 4L SORP cell sorter (Becton Dickinson) The purity of the sorted microglial cells was above
632 90%.
633
634 *Primary neuronal culture:*
635 Primary neuronal cultures were prepared from E17 pregnant mice of CD1 background (Janvier Labs,
636 France). Briefly, mice were sacrificed and the brains of embryos were taken out, meninges removed,
637 and the cortex dissected out. The cortexes were washed in 1× PBS (Pan Biotech, Germany). Single-cell
638 suspensions were generated by incubating them with trypsin and DNase before careful disintegration.
639 One hundred and thirty thousand cells per well were plated on poly-D-lysine-coated 24-well plates in
640 Neurobasal medium (Thermo Fisher Scientific, Germany) supplemented with B-27 (Thermo Fisher
641 Scientific, Germany). Primary cortical neurons were used for experiments at DIV10-12.
642
643 *Cell lines*
644 All human iPSCs used in this study are commercially available and reported to be derived from material
645 obtained under informed consent and appropriate ethical approvals.
646
647 *Differentiation of microglia from induced pluripotent stem cells:*

648 Human induced pluripotent stem cells lines (hiPSCs) (Cell line IDs: KOLF2.1J [93] were obtained from
649 The Jackson Laboratory; BIONi010-C and BIONi037-A were both from the European bank for Induced
650 Pluripotent Stem Cells) were differentiated to microglia as previously described [94]. In brief, 3 x 10^6
651 iPSCs were seeded into an Aggrewell 800 well (STEMCELL Technologies) to form embryoid bodies
652 (EBs), in mTeSR1 and fed daily with medium plus 50 ng/ml BMP4 (Miltenyi Biotec), 50 ng/ml VEGF
653 (Miltenyi Biotec), and 20 ng/ml SCF (R&D Systems). Four-day EBs were then differentiated in 6-well
654 plates (15 EBs/well) in X-VIVO15 (Lonza) supplemented with 100 ng/ml M-CSF (Miltenyi Biotec), 25
655 ng/ml IL-3 (Miltenyi Biotec), 2 mM Glutamax (Invitrogen Life Technologies), and 0.055 mM beta-
656 mercaptoethanol (Thermo Fisher Scientific), with fresh medium added weekly. Microglial precursors
657 emerging in the supernatant after approximately 1 month were collected and isolated through a 40
658 um cell strainer and plated in N2B27 media supplemented with 100 ng/ml M-CSF, 25 ng/ml interleukin
659 34 (IL-34) for differentiation.
660
661 Q*uantitative PCR experiment:*
662 cDNA synthesis was performed using the miScript II RT Kit (Qiagen, Germany) according to the
663 manufacturer's protocol. In brief, 200 ng total RNA was used for cDNA preparation. HiFlex Buffer was
664 used so that the cDNA could be used for both mRNA and microRNA quantitative PCR (qPCR). A
665 microRNA-specific forward primer and a universal reverse primer were used for quantification. The
666 U6 small nuclear RNA gene was employed as an internal control. For mRNA quantification, gene-
667 specific forward and reverse primers were used. The relative amounts of mRNA were normalized
668 against GAPDH. The fold change for each microRNA and mRNA was calculated using the 2–ΔΔCt
669 method[18]. The Light Cycler® 480 Real-Time PCR System (Roche, Germany) was used to perform qPCR.
670
671 *Caspase 1 activation assay:*
672 Caspase-Glo® 1 Inflammasome Assay (Promega, Germany) was used to detect caspase 1 activation as
673 described in the manufacturer's protocol. In brief, microglia, treated with ASO/inhibitor or primed
674 with LPS and stimulated with ATP, were seeded on opaque, flat-bottom 96-well plates (Cellstar,
675 Germany) at 50,000 per well in 100 ul DMEM supplemented with 10% FBS, 20% L929 conditioned
676 medium and 100 U ml–1 penicillin–streptomycin. 100 ul of Caspase-Glo buffer was mixed with cell
677 medium. Plates were incubated at room temperature for 1 h. Luminogenic caspase activity was
678 measured using a FLUOstar Omega plate reader (BMG Labtech).
679
680 *Microglia phagocytosis assay:*

681 The microglia phagocytosis assay was performed as described[19]. Primary microglia cultures were
682 plated at a density of 18 x 10^4 in poly-D-lysine-coated 24-well plates in DMEM supplemented with 10%
683 FBS, 20% L929 conditioned medium and 100 U ml–1 penicillin–streptomycin. Immortalized microglia
684 (IMG) cultures were plated at a density 5 x 10^3 in poly-D-lysine-coated 24-well plates in DMEM
685 supplemented with 10% FBS, 1X Glutamine (Millipore), and 100 U ml–1 penicillin–streptomycin. To
686 evaluate phagocytosis, treated microglia were incubated with fluorescent latex beads of 1 µm
687 diameter (green, fluorescent 496/519; Sigma-Aldrich) for 1 h at 37°C, rinsed, and fixed with 4%
688 formaldehyde. Cells were stained using the Iba1 (CD68) antibody (1:500; Wako) and DAPI. A confocal
689 microscope was used for imaging at a low magnification (10x). ImageJ was used to quantify fluorescent
690 latex beads. Region of interests (ROIs) were selected as microglial cells outlined with the Iba1
691 immunostaining to quantify beads. An intracellular section of the cell was selected to assure
692 engulfment of latex beads by microglia. Similar acquisition parameters were used for each individual
693 experiment. The results were expressed as the percentage of phagocytic index (# of total engulfed
694 beads in an image / # of total cells identified in an image; n = 13 independent experiments).
695
696 *Synaptic pruning in primary microglia neural co-culture:*
697 Primary cortical neurons were seeded at a density of 130,000 on poly-D-lysine-coated 13 mm
698 coverslips in 24-well plates in Neurobasal medium supplemented with B-27. Primary cortical neurons
699 were used for experiments at DIV10-12. Treated primary microglia cultures were harvested from T-75
700 flasks and 4000 cells were seeded to each neural culture well. Plates were kept at 37°C for three days.
701 On the third day, the cells were washed and fixed with 4% PFA (Sigma Aldrich, Germany) and 100
702 mM NH4Cl (Merck, Germany) respectively, at room temperature for 30 minutes. Next, the cells were
703 washed in permeabilization and blocking buffer (0.1% Triton-X [Merck, Germany] + 3% bovine serum
704 albumin (BSA) [AppliChem GmbH, Germany]) on a shaker. The cells were then incubated with primary
705 antibodies for 1 hour at room temperature. The antibodies used included synaptophysin 1 (guinea pig,
706 SySy), PSD-95 (rabbit, Cell Signaling,), and Iba1 (goat, Abcam). After incubation, the cells were washed
707 in PBS and then incubated with a secondary antibody for 1 hour at room temperature. As secondary
708 antibodies, Cy3 (donkey, anti- guinea pig, Jackson Imm.), Abberrior STAR 635p (goat, anti-rabbit) were
709 used. Mowiol (Merck, Germany) and DAPI were used as a mounting medium. Images were taken with
710 a multicolor confocal STED microscope (Abberior Instruments GmbH, Göttingen, Germany). Analysis
711 of colocalization of pre- and post-synaptic markers were performed using SynQuant plugins in Fiji (v
712 2.0.0).
713
714 *Dendritic spine analysis:*

715 As described above, primary cortical neurons and primary microglia were co-cultured and fixed with
716 4%PFA. Dendritic spines were labeled as described [95]. In brief, the cells were aspirated and 2-3
717 crystals of Dil stain (Life Technologies-Molecular Probes) were added to each culture well and
718 incubated on a shaker for 10 minutes at room temperature. Cells were washed with PBS until no
719 crystals were visible and incubated overnight at room temperature. On the following day, the cells
720 were washed and mounted with Mowiol. For high-magnification images, a multicolor confocal STED
721 microscope with a 60× oil objective was used. Spine density and total spine length were measured by
722 using ImageJ.
723
724 *Protein extraction of primary microglia:*
725 Primary microglia cell lysates were used to detect ZBP1 in RIPA fractions. Primary microglia were
726 seeded in a 6-well plate at a density of 1 x 10^6 in each well. Cells were collected in a RIPA buffer
727 supplemented with 1 x protease inhibitor. Samples were kept on ice for 15 minutes and vortexed
728 every 5 minutes and then centrifuged at 5000 rpm for 15 minutes at 4°C before supernatants were
729 transferred to a new tube and stored at –20°C. The protein concentration was measured using a BCA
730 assay.
731
732 *Immunoblot analysis:*
733 For standard immunoblot analysis, 20 ug of samples were mixed with 1× Laemmli buffer (Sigma,
734 Germany), heated for 5 min at 95°C and loaded onto 4–15% Mini-PROTEAN® TGX™ Precast Protein
735 Gels (Bio-Rad, Germany). Proteins were transferred on nitrocellulose membranes and membranes
736 were blocked with 5% BSA in PBS-Tween. Membranes were incubated with primary antibodies in 5%
737 BSA in PBS-Tween. Fluorescent-tagged secondary antibodies (LI-COR) were used for visualization of
738 proteins. Imaging was performed using a LI-COR ODYSSEY. HSP-70, GAPDH were used as a loading and
739 run on the same gel.
740
741 *Treatment of microglia:*
742 Microglia activation by LPS was used as a positive control. For this, microglia cells were first primed
743 with 100 ng/ml ultrapure LPS (E. coli 0111:B4, Invivogen) and then incubated at 37°C. After this, 5 mM
744 ATP were added to the culture and incubated for 30 minutes. Caspase 1 assay and phagocytosis assay
745 were performed from these cultures. For immunoblot, cell lysate was prepared. For miR99b-5p-
746 related analysis, microglia were either treated for two days with miR99b-5p inhibitor/negative control
747 or ASOs in T-75 after first harvesting or after harvesting cells were seeded in a 24-well culture plate.
748

749 *Luciferase assay:*

750 Seed sequences of miR-99b-5p and pairing 3'UTR sequences of Zbp1 were generated with TargetScan.
751 Cloned 3'UTR sequence of Zbp1 and scrambles UTR were purchased from Gene Copoeia
752 (https://www.genecopoeia.com/product/mirna-target-clones/mirna-targets/). UTR was cloned
753 downstream to firefly luciferase of pEZX-MT06 Dual-Luciferase miTarget™ vector. The pEZX-MT06-
754 scrambled UTR or pEZX-MT06-Zbp1 3'UTR construct and miR99b-5p mimic or negative control were
755 co-transfected into HEK293-T cells cultured in 24-well plates using EndoFectin™ Max Transfection
756 Reagents (Gene Copoeia) according to the manufacturer's protocol. 48 hours after transfection, Firefly
757 and Renilla luciferase activities were measured using a Luc-Pair™ Duo-Luciferase HS Assay Kit (for high
758 sensitivity) (GeneCopoeia). Firefly luciferase activity and Renilla luciferase activity were normalized.
759 The mean of luciferase activity and of Firefly/Renilla was considered for the analysis.

760

761 *Statistical analysis:*

762 Unless otherwise noted, statistical analysis was carried out with GraphPad Prism software version 8.0.
763 Statistical measurement is shown as mean ± SD. Each n represents a biological sample. Either a two-
764 tailed unpaired t-test or a two-way ANOVA with Tukey's post hoc test were applied to analyze the
765 data. Enriched gene ontology and pathway analysis was performed using Fisher's exact test followed
766 by a Benjamini-Hochberg correction.

767

768 **Conflict of interest**

769 The authors declare no conflict of interest.

770

771 **Acknowledgment**

772 This work was supported by the following grants to AF: The DFG (*Deutsche Forschungsgemeinschaft*)
773 priority program 1738, SFB1286, the EPIFUS project, Germany's Excellence Strategy - EXC 2067/1
774 390729940. FS was supported by the GoBIO project miRassay. Urs Heilbronner is supported by the
775 European Union's Horizon 2020 Research and Innovation Programme (PSY-PGx, grant agreement No
776 945151) and the Deutsche Forschungsgemeinschaft (DFG, German Research Foundation, project
777 number 514201724). LE is supported by the Studienstiftung des Deutschen Volkes and the
778 International Max-Planck Research School for The Mechanisms of Mental Function and Dysfunction
779 (IMPRS-MMFD). DKV is supported by grants from the Chan Zuckerberg Initiative Neurodegenerative's
780 Challenge Network (2020-221779(5022) & 2021-235147). TS was supported by grants from
781 the *Deutsche Forschungsgemeinschaft* (DFG; SCHU 1603/4-1, 5-1, 7-1), the German Ministry of

782 Education and Research (BMBF; 01EE1404H), and the Dr. Lisa Oehler Foundation (Kassel, Germany).
783 PF was supported by a grant from the DFG (DFG; FA 241/16-1)
784
785 **Author contributions:** L.K., F.S., and A.F. designed research; L.K., M.R.I., J.Z., J.S., R.P., S.B., L.E., A.B.,
786 D.K.V., I.D., F.O., and A.F. performed research; U.H., A.B., M.B., F.S., M.O.K., E.C.S., M.S., E.Z.R., G.J.,
787 T.G.S., P.F. recruited and phenotyped patients; L.K., M.R.I., D.M.K., A.M., T.P., and A.F. analyzed data;
788 and L.K., F.S., and A.F. wrote the paper with input from other co-authors.
789
790 **Figure legends**
791 **Figure 1: Identification of microRNAs that play a role in the pathogenesis of SZ. a.** Experimental
792 scheme. **b.** Violin plots showing the results of WGCNA analysis. Depicted is the comparison of the
793 eigenexpression in of the 3 co-expression modules in SZ patients and in control, showing a decrease
794 in SZ patients. **c.** Violin plots showing the results of WGCNA analysis. The eigenexpression of the 5 co-
795 expression modules was higher in SZ patients than in controls (for b & c: unpaired t test; **P < 0.01,
796 ***P < 0.001; ****P < 0.0001, a P value < 0.01 was considered as significant). **d.** Heat map showing
797 the correlation of the eigenexpression of the co-expression modules shown in (a) and (b) with the
798 corresponding clinical phenotypes. The numbers in each rectangle represent the correlation (upper
799 number) and the corresponding p-value (lower number). A P value < 0.01 was considered as
800 significant. **e.** Volcano plot depicting the results of the differential expression analysis when comparing
801 SZ patients and controls shown in (a). **f.** Volcano plot demonstrating the results of the differential
802 expression when comparing postmortem brain samples from SZ patients (n=13) and controls (n=17).
803 **g.** Venn diagram comparing the microRNAs detected in blood samples when performing differential
804 expression analysis (Blood DESEQ2_DE), the microRNAs of the ME_Turquoise and ME_Pink co-
805 expression modules and the microRNAs differentially expressed when comparing postmortem brain
806 tissue (brain_DE). miR-99b-5p is the only microRNA decreased in all comparisons. **h.** Heat map
807 showing the correlation of miR-99b-5p expression levels to the clinical phenotypes for the individuals
808 as analyzed in (a). The numbers in each rectangle represent the correlation (upper number) and the
809 corresponding p-value (lower number).
810
811 **Figure 2: Decreasing miR-99b-5p levels in the PFC of mice leads to SZ-like phenotypes and increases**
812 **the expression of genes linked to microglia activation. a.** Left panel: Experimental design. Right panel:
813 Bar graph showing qPCR results for miR-99b-5p in tissue obtained from the PCF of mice 5 or 10 days
814 after injection of anti-miR-99b or sc-control oligonucleotides. (n=4/group; ****P < 0.0001, unpaired t
815 test). **b**. Bar graph showing the distance traveled in the open field test of mice injected to the PFC with

816 either anti-miR-99b or sc-control oligonucleotides (n=10/group; unpaired t test. **c.** Bar graph showing
817 the time spent in the center of the open field in mice injected to the PFC with either anti-miR-99b or
818 sc-control oligonucleotides (n=10/group; *P < 0.05; unpaired t test). **d.** Bar graph showing the time
819 spent in the open arms when an elevated plus maze test was performed in mice injected to the PFC
820 with either anti-miR-99b or sc-control oligonucleotides (n=10/group; *P < 0.05; unpaired t test). **e.** Bar
821 graph showing the results of a PPI experiment of mice injected with either anti-miR-99b or sc-control
822 oligonucleotides. PPI is impaired in anti-miR-99b injected mice (n=10/group) unpaired t test; *P < 0.05;
823 **P < 0.01, ***P < 0.001; ****P < 0.0001). **f.** Bar graph showing the basic startle response among
824 groups. **g.** Volcano plot showing the differentially expressed genes (upregulated in red, downregulated
825 in blue) when RNA-seq was performed from the PFC of mice injected with either anti-miR-99b or sc-
826 control oligonucleotides. Genes with log2-fold change ± 0.5 and adjusted p value < 0.05 are
827 highlighted. **h.** GO-term analysis of the upregulated genes found in (e). **i.** Heat maps showing the
828 enrichment of the upregulated genes as determined in (e) in various datasets. Left panel shows that
829 the upregulated genes are enriched for microglia-specific genes, while the downregulated genes are
830 enriched for neuron-specific genes. The right panel shows that the upregulated genes are over-
831 represented in 3 different databases for immune function-related genes. **j.** Bar graph showing the
832 qPCR results of the *Il1ß*, *Tgfb1* and *Tnfa* genes in FACS-sorted microglia collected from the PFC of mice
833 injected with anti-miR-99b or sc-control oligonucleotides. (n=4 or 5/group; unpaired t test; *P < 0.05).
834 Error bars indicate SD.
835
836 **Figure 3: Decreasing miR-99b-5p levels in microglia increases phagocytosis and reduces synapse**
837 **number in cortical neurons a.** Left panel: Experimental design. **b.** Volcano plot showing differential
838 expressed genes when comparing microglia treated with anti-miR-99b or sc-control LNAs. Genes with
839 statistical significance are highlighted. **c.** Bar chart showing the top GO terms represented by the up
840 regulated genes shown in (b). **d.** Bar charts showing qPCR results for *Tgfb1*, *Il1ß* and *Tnfa* comparing
841 microglia treated with anti-miR-99b or sc-control LNAs (n=6/group; unpaired t test; *P < 0.05;
842 **P < 0.01, ****P < 0.0001). **e.** Bar chart showing the results of a phagocytosis assay performed in
843 microglia treated with anti-miR-99b in comparison to cells treated with sc-control LNAs. The
844 percentage of phagocytic index represents (# of total engulfed beads in an image / # of total cells
845 identified in an image; n = 13 independent experiments; unpaired t test; **P < 0.01). **f**. Experimental
846 scheme illustrating the co-culture experiment. **g.** Heat map showing the differentially expressed genes
847 from the experiment described in (f). **h.** Plot showing the results of a GO term analysis for the up- and
848 downregulated genes displayed in (g). **i.** Left panel: Representative image showing DIL dye staining to
849 visualize dendritic spines in co-cultures as illustrated in (f). Scale bar 5 µm. Right panel: Bar chart

850 showing the statistical quantification of the data depicted in (i). Each dot represents a spine density
851 for a dendritic segment. *P < 0.05; **P < 0.01, ***P < 0.001; ****P < 0.0001). Error bars indicate SD.
852
853 **Figure 4: miR-99b-5p regulates neuroinflammatory phenotypes via *Zbp1* a.** Venn diagram comparing
854 the genes upregulated in the PFC of mice and in primary microglia when injected or treated with anti-
855 miR99b vs. sc-control LNAs, respectively. The data is further compared to the identified 13 miR-99b-
856 5p target mRNAs detected in the PFC dataset. The left panel shows the gene names of the 13 miR-
857 99b-5p target mRNAs. Red indicates miR-99b-5p targets upregulated in the PCF and in primary
858 microglia upon anti-miR-99b treatment. **b.** Bar graph showing the results of the luciferase assay. In
859 comparison to sc-control LNAs, administration of miR-99b-5p mimic decreases luciferase activity when
860 cells express the Zbp1-3'UTR. This effect is not observed when a control 3'UTR that does not bind miR-
861 99b-5p is used. (n=6/group). The upper right panel shows the predicted binding of miR-99b-5p to the
862 3'UTR of *Zbp1*. **c.** Left panel: Representative immunoblot image showing ZBP1 levels in microglia
863 treated with sc-control LNAs or anti-miR-99b. HSP70 was used as a loading control. Right panel: Bar
864 graph showing the quantification of the data depicted in the left panel. n=4/group. **d.** Bar graph
865 showing quantification of caspase activity in primary microglia treated with sc-control LNAs or anti-
866 miR-99b (n=6/group). **e.** Bar graph showing quantification of caspase activity in protein lysates
867 isolated from the PFC of mice injected with anti-miR-99b or sc-control (n=4/group). **f.** Bar graph
868 showing quantification of caspase activity in primary microglia treated with either sc-control LNAs,
869 anti-miR-99b or anti-miR-99b together with *Zbp1*-ASOs. (n=6/group). **g.** Bar graph showing qPCR
870 results for *Il1ß* in primary microglia treated with either sc-control LNAs, anti-miR-99b or anti-miR-99b
871 together with *Zbp1*-ASOs (n=6/group). **h.** Bar graph showing the results of a phagocytosis assay
872 performed in primary microglia treated with either sc-control LNAs, anti-miR-99b or anti-miR-99b
873 together with *Zbp1*-ASOs (n=16 independent experiments). **i.** Bar graph showing quantification of
874 caspase activity in human iPSC-derived microglia treated with either sc-control LNAs, anti-miR-99b or
875 anti-miR-99b together with *Zbp1*-ASOs (n=13-16 samples/group). **j.** Bar graph showing qPCR results
876 for IL1ß in human iPSC-derived microglia treated with either sc-control LNAs, anti-miR-99b or anti-
877 miR-99b together with *Zbp1*-ASOs (n=6/group). **k.** Bar graph showing the results of a phagocytosis
878 assay performed in human iPSC-derived microglia treated with either sc-control LNAs, anti-miR-99b
879 or anti-miR-99b together with *Zbp1*-ASOs. The percentage of phagocytic index represent (# of total
880 engulfed beads in an image / # of total cells identified in an image; n = 9 independent experiments.
881 Error bars indicate SD; unpaired t test; *P < 0.05; **P < 0.01, ***P < 0.001; ****P < 0.0001). RI: relative
882 immunofluorescent,
883

884 **References**

885

886 [1] R. C. Kessler, W. T. Chiu, O. Demler, K. R. Merikangas, and E. E. Walters, "Prevalence,
887 severity, and comorbidity of 12-month DSM-IV disorders in the National Comorbidity
888 Survey Replication," *Arch. Gen. Psychiatry,* vol. 62, no. 617-627, 2005.
889 [2] K. Jaeschke, F. Hanna, S. Ali, N. Chowdhary, T. Dua, and F. Charlson, "Global estimates
890 of service coverage for severe mental disorders: findings from the WHO Mental Health
891 Atlas 2017," *Ment Health (Camb),* vol. 21, no. 8, p. e27, 2021.
892 [3] E. J. Nestler, C. J. Peña, M. Kundakovic, A. Mitchell, and S. Akbarian, "Epigenetic Basis
893 of Mental Illness.," *Neuroscientist,* vol. 8, no. Epub ahead of print], 2015.
894 [4] I. Giegling *et al.*, "Genetics of schizophrenia: A consensus paper of the WFSBP Task
895 Force on Genetics.," *World J Biol Psychiatry.,* vol. 18, no. 7, pp. 492-505, 2017.
896 [5] N. Robinson and S. E. Bergen, "Environmental Risk Factors for Schizophrenia and
897 Bipolar Disorder and Their Relationship to Genetic Risk: Current Knowledge and
898 Future Directions," *Front Genet.,* vol. 28, no. 12, p. 686666, 2021.
899 [6] M. T. Samara *et al.*, "Efficacy, Acceptability, and Tolerability of Antipsychotics in
900 Treatment-Resistant Schizophrenia: A Network Meta-analysis.," *JAMA Psychiatry,* vol.
901 73, no. 3, pp. 199-210, 2016.
902 [7] D. L. Spark, A. Fornito, C. J. Langmead, and G. D. Stewart, "Beyond antipsychotics: a
903 twenty-first century update for preclinical development of schizophrenia
904 therapeutics," *Transl Psychiatry.,* vol. 7, no. 12, p. 147, 2022.
905 [8] I. Ezkurdia *et al.*, "Multiple evidence strands suggest that there may be as few as
906 19,000 human protein-coding genes.," *Hum Mol Genet.,* vol. 23, no. 22, pp. 5866-
907 5878, 2014.
908 [9] T. R. Damase, R. Sukhovershin, C. Boada, F. Taraballi, R. I. Pettigrew, and J. P. Cooke,
909 "The Limitless Future of RNA Therapeutics.," *Front Bioeng Biotechnol.,* vol. 18, no. 9,
910 p. 628137, 2021.
911 [10] R. Feng, S. Patil, X. Zhao, Z. Miao, and A. Qian, "RNA Therapeutics - Research and
912 Clinical Advancements," *Front Mol Biosci.,* vol. 22, no. 8, p. 710738, 2021.
913 [11] R. Rupaimoole and F. Slack, J. , "MicroRNA therapeutics: towards a new era for the
914 management of cancer and other diseases.," *Nat Rev Drug Discov.,* vol. 16, no. 3, pp.
915 203-222, 2017.
916 [12] A. M. Gurtan and P. A. Sharp, "The Role of miRNAs in Regulating Gene Expression
917 Networks.," *J Mol Biol,* vol. pii, no. S0022-2836(13)00154-X., p. Epub ahead of print,
918 2013.
919 [13] C. Bär *et al.*, "Non-coding RNAs: update on mechanisms and therapeutic targets from
920 the ESC Working Groups of Myocardial Function and Cellular Biology of the Heart.,"
921 *Cardiovasc Res.,* vol. 116, no. 11, pp. 1805-1819, 2020.
922 [14] A. Fischer, "Epigenetic memory: the Lamarckian brain.," *EMBO J,* vol. 33, no. 9, pp.
923 945-967, 2014.
924 [15] H. C. Martins and G. Schratt, "MicroRNA-dependent control of neuroplasticity in
925 affective disorders.," *Transl Psychiatry.,* vol. 11, no. 1, p. 263, 2021.
926 [16] K. Sakamoto and J. J. Crowley, "A comprehensive review of the genetic and biological
927 evidence supports a role for MicroRNA-137 in the etiology of schizophrenia," *Am J*
928 *Med Genet B Neuropsychiatr Genet.,* vol. 177, no. 2, pp. 242-256, 2017.

929 [17] S. Sargazi *et al.*, "Functional Variants of miR-143 Are Associated with Schizophrenia
930 Susceptibility: A Preliminary Population-Based Study and Bioinformatics Analysis.,"
931 *Biochem Genet.,* vol. 60, no. 3, pp. 868-881, 2022.
932 [18] B. Roy, Y. Yoshino, L. Allen, K. Prall, G. Schell, and Y. Dwivedi, "Exploiting Circulating
933 MicroRNAs as Biomarkers in Psychiatric Disorders.," *Molecular diagnosis & therapy,*
934 vol. 24, no. 3, pp. 279-298, 2020.
935 [19] S. Ghafouri-Fard, R. Eghtedarian, M. Taheri, A. Beatrix Brühl, D. Sadeghi-Bahmani, and
936 S. A. Brand, "Review on the Expression Pattern of Non-coding RNAs in Patients With
937 Schizophrenia: With a Special Focus on Peripheral Blood as a Source of Expression
938 Analysis.," *Front Psychiatry.,* vol. 18, no. 12, p. 640463, 2021.
939 [20] E. E. Tsermpini, C. I. Kalogirou, G. C. Kyriakopoulos, G. P. Patrinos, and C. Stathopoulos,
940 "miRNAs as potential diagnostic biomarkers and pharmacogenomic indicators in
941 psychiatric disorders.," *Pharmacogenomics J.,* vol. 22, no. 4, pp. 211-222, 2022.
942 [21] W. Liang *et al.*, "Loss of schizophrenia-related miR-501-3p in mice impairs sociability
943 and memory by enhancing mGluR5-mediated glutamatergic transmission.," *Sci Adv,*
944 vol. 8, no. 33, p. eabn7357, 2022.
945 [22] A. Zampetaki, P. Willeit, I. Drozdov, S. Kiechl, and M. Mayr, "Profiling of circulating
946 microRNAs: from single biomarkers to re-wired networks.," *Cardiovascular research,*
947 vol. 93, no. 4, pp. 555–562., 2012.
948 [23] C. E. Condrat *et al.*, "miRNAs as Biomarkers in Disease: Latest Findings Regarding Their
949 Role in Diagnosis and Prognosis.," *Cells,* vol. 9, no. 2, p. 276, 2020.
950 [24] A. M. Jose, "Movement of regulatory RNA between animal cells.," *Genesis,* vol. 53, no.
951 7, pp. 395-416, 2015.
952 [25] R. Bayraktar, K. Van Roosbroeck, and G. A. Calin, "Cell-to-cell communication:
953 microRNAs as hormones," *Mol Oncol.,* vol. 11, no. 12, pp. 1673-1686., 2017.
954 [26] M. Budde *et al.*, "A longitudinal approach to biological psychiatric research: The
955 PsyCourse study.," *Am J Med Genet B Neuropsychiatr Genet.,* vol. 180, no. 2, pp. 89-
956 102, 2018.
957 [27] T. Kuriakose and T. D. Kanneganti, "ZBP1: Innate Sensor Regulating Cell Death and
958 Inflammation.," *Trends Immunol.,* vol. 39, no. 2, pp. 123-134, 2018.
959 [28] E. A. Ermakov, M. M. Melamud, V. N. Buneva, and S. A. Ivanova, "Immune System
960 Abnormalities in Schizophrenia: An Integrative View and Translational Perspectives.,"
961 *Front Psychiatry.,* vol. 25, no. 13, p. 880568, 2022.
962 [29] S. Liu *et al.*, "Diagnostic value of blood-derived microRNAs for schizophrenia: results
963 of a meta-analysis and validation.," *Scientific reports,* vol. 7, no. 1, p. 15328, 2017.
964 [30] A. M. Achim, M. Maziade, E. Raymond, D. Olivier, C. Mérette, and M. A. Roy, "How
965 prevalent are anxiety disorders in schizophrenia? A meta-analysis and critical review
966 on a significant association.," *Schizophr Bull.,* vol. 37, no. 4, pp. 811-821, 2011.
967 [31] N. R. Swerdlow, D. L. Braff, N. Taaid, and M. A. Geyer, "Assessing the validity of an
968 animal model of deficient sensorimotor gating in schizophrenic patients," *Arch Gen*
969 *Psychiatry,* vol. 51, no. 2, pp. 139-154, 1994.
970 [32] G. A. Light and D. L. Braff, "Human and animal studies of schizophrenia-related gating
971 deficits.," *Curr Psychiatry Rep.,* vol. 1, no. 1, pp. 31-40, 1999.
972 [33] M. van den Buuse, "Modeling the positive symptoms of schizophrenia in genetically
973 modified mice: pharmacology and methodology aspects.," *Schizophr Bull.,* vol. 36, no.
974 2, pp. 246-270, 2010.

[34] R. Rahimian, M. Wakid, L. A. O'Leary, and N. Mechawar, "The emerging tale of microglia in psychiatric disorders.," *Neurosci Biobehav Rev.,* vol. 131, pp. 1-29, 2021.

[35] K. Borst, A. A. Dumas, and M. Prinz, "Microglia: Immune and non-immune functions," *Immunity.,* vol. 54, no. 10, pp. 2194-2208, 2021.

[36] C. M. Sellgren *et al.*, "Increased synapse elimination by microglia in schizophrenia patient-derived models of synaptic pruning.," *Nat Neurosci.,* vol. 22, no. 3, p. 374, 2019.

[37] N. Müller, E. Weidinger, B. Leitner, and M. J. Schwarz, "The role of inflammation in schizophrenia.," *Front Neurosci.,* vol. 21, no. 9, p. 372, 2015.

[38] H. C. van Mierlo, A. Schot, M. P. M. Boks, and L. D. de Witte, "The association between schizophrenia and the immune system: Review of the evidence from unbiased 'omic-studies'." *Schizophr Res.,* vol. 217, no. 114-123, 2020.

[39] R. P. Sharma, C. Rosen, J. K. Melbourne, B. Feiner, and K. A. Chase, "2016," *Neuroimmunomodulation,* vol. 23, no. 4, pp. 224-229.

[40] H. I. Muendlein *et al.*, "ZBP1 promotes LPS-induced cell death and IL-1β release via RHIM-mediated interactions with RIPK1," *Nat Commun.,* vol. 12, no. 1, p. 86, 2021.

[41] R. G. Shao *et al.*, "Necrostatin-1 attenuates Caspase-1-dependent pyroptosis induced by the RIPK1/ZBP1 pathway in ventilator-induced lung injury," *Cytokine,* vol. 157, p. 155950, 2022.

[42] R. de Reuver *et al.*, "ADAR1 prevents autoinflammation by suppressing spontaneous ZBP1 activation," *Nature,* vol. 607, no. 7920, pp. 784-789, 2022.

[43] P. F. Buckley, "Neuroinflammation and Schizophrenia," *Curr Psychiatry Rep,* vol. 21, no. 8, p. 72, 2019.

[44] A. C. Rodrigues-Neves, A. F. Ambrósio, and C. A. Gomes, "Microglia sequelae: brain signature of innate immunity in schizophrenia.," *Transl Psychiatry.,* vol. 12, no. 1, p. 493, 2022.

[45] C. Barbato *et al.*, "Cognitive Decline and Modulation of Alzheimer's Disease-Related Genes After Inhibition of MicroRNA-101 in Mouse Hippocampal Neurons," *Molecular Neurobiology,* vol. 57, no. 7, pp. 3183-3194, 2020.

[46] M. Mundalil Vasu *et al.*, "Serum microRNA profiles in children with autism.," *Molecular autism,* vol. 5, no. 40, pp. https://doi.org/10.1186/2040-2392-5-40, 2014.

[47] F. Zadehbagheri, E. Hosseini, Z. Bagheri-Hosseinabadi, H. M. Rekabdarkolaee, and I. Sadeghi, "Profiling of miRNAs in serum of children with attention-deficit hyperactivity disorder shows significant alterations," *Journal of psychiatric research,* vol. 109, pp. 185-192, 2019.

[48] H. Zhu and S. W. Leung, "MicroRNA biomarkers of type 2 diabetes: evidence synthesis from meta-analyses and pathway modelling," *Diabetologia,* vol. 66, no. 2, pp. 288-299, 2023.

[49] S. Y. Zahari Sham *et al.*, "Circulating miRNAs in Type 2 Diabetic Patients with and without Albuminuria in Malaysia.," *Kidney & blood pressure research,* vol. 47, no. 2, pp. 81-93, 2022.

[50] F. Moshiri *et al.*, "Circulating miR-106b-3p, miR-101-3p and miR-1246 as diagnostic biomarkers of hepatocellular carcinoma," *Oncotarget,* vol. 9, no. 20, pp. 15350-15364, 2018.

[51] Y. Zhang, P. Zhang, and C. Deng, "miR-378a-5p regulates CAMKK2/AMPK pathway to contribute to cerebral ischemia/reperfusion injury-induced neuronal apoptosis.," *Folia histochemica et cytobiologica,* vol. 59, no. 1, pp. 57-65, 2021.

1022 [52] J. M. Biselli *et al.*, "Differential microRNA expression profile in blood of children with
1023 Down syndrome suggests a role in immunological dysfunction.," *Human cell,* vol. 35,
1024 no. 2, pp. 639-648, 2022.
1025 [53] Z. Dong *et al.*, "Profiling of Serum Exosome MiRNA Reveals the Potential of a MiRNA
1026 Panel as Diagnostic Biomarker for Alzheimer's Disease.," *Molecular Neurobiology,* vol.
1027 58, no. 7, pp. 3084-3094, 2021.
1028 [54] S. D. Chen *et al.*, "A preliminary analysis of microRNA-21 expression alteration after
1029 antipsychotic treatment in patients with schizophrenia," *Psychiatry research,* vol. 244,
1030 pp. 324-332, 2016.
1031 [55] E. Maffioletti *et al.*, "Peripheral whole blood microRNA alterations in major depression
1032 and bipolar disorder.," *Journal of affective disorders,* vol. 200, pp. 250-258, 2016.
1033 [56] J. Vykoukal *et al.*, "Contributions of Circulating microRNAs for Early Detection of Lung
1034 Cancer," *Cancers,* vol. 14, no. 17, p. 4221, 2022.
1035 [57] Z. Qin, X. Han, J. Ran, S. Guo, and L. Lv, "Exercise-Mediated Alteration of miR-192-5p
1036 Is Associated with Cognitive Improvement in Alzheimer's Disease,"
1037 *Neuroimmunomodulation,* vol. 29, no. 1, pp. 36-43, 2022.
1038 [58] Y. Yoshino, B. Roy, and Y. Dwivedi, "Differential and unique patterns of synaptic miRNA
1039 expression in dorsolateral prefrontal cortex of depressed subjects.,"
1040 *Neuropsychopharmacology,* vol. 46, no. 5, pp. 900-910, 2021.
1041 [59] C. Z. Tang, J. T. Yang, Q. H. Liu, Y. R. Wang, and W. S. Wang, "Up-regulated miR-192-
1042 5p expression rescues cognitive impairment and restores neural function in mice with
1043 depression via the Fbln2-mediated TGF-β1 signaling pathway," *FASEB J,* vol. 33, no. 1,
1044 pp. 606-618, 2019.
1045 [60] S. Van der Auwera *et al.*, "Association of childhood traumatization and
1046 neuropsychiatric outcomes with altered plasma micro RNA-levels.,"
1047 *Neuropsychopharmacology,* vol. 44, no. 12, pp. 2030-2037, 2019.
1048 [61] Z. X. Huang, Y. Chen, H. R. Guo, and G. F. Chen, "Systematic Review and Bioinformatic
1049 Analysis of microRNA Expression in Autism Spectrum Disorder Identifies Pathways
1050 Associated With Cancer, Metabolism, Cell Signaling, and Cell Adhesion," *Frontiers in*
1051 *Psychiatry,* vol. 12, p. 630876, 2021.
1052 [62] E. Banach, A. Szczepankiewicz, L. Kaczmarek, T. Jaworski, and J. Urban-Ciećko,
1053 "Dysregulation of miRNAs Levels in Glycogen Synthase Kinase-3β Overexpressing Mice
1054 and the Role of miR-221-5p in Synaptic Function," *Neuroscience,* vol. 490, no. 10, pp.
1055 287-295, 2022.
1056 [63] S. van Heukelum *et al.*, "Where is Cingulate Cortex? A Cross-Species View.," *Trends*
1057 *Neurosci.,* vol. 43, no. 5, pp. 285-299, 2020.
1058 [64] D. Feifel and P. D. Shilling, "Promise and pitfalls of animal models of schizophrenia.,"
1059 *Psychiatry Rep,* vol. 12, pp. 327-334, 2010.
1060 [65] T. A. Bayer, R. Buslei, L. Havas, and P. Falkai, "Evidence for activation of microglia in
1061 patients with psychiatric illnesses," *Neurosci Lett.,* vol. 271, no. 2, pp. 126-128, 1999.
1062 [66] M. E. Benros, P. R. Nielsen, M. Nordentoft, W. W. Eaton, S. O. Dalton, and P. B.
1063 Mortensen, "Autoimmune diseases and severe infections as risk factors for
1064 schizophrenia: a
1065 30-year population-based register study," *Am J Psychiatry,* vol. 168, no. 1303-1310, 2011.
1066 [67] B. N. van Berckel, M. G. Bossong, R. Boellaard, R. Kloet, A. Schuitemaker, and E.
1067 Caspers, "Microglia activation in recent-onset schizophrenia: a quantitative (R)-

[11 C]PK11195 positron emission tomography study.," *Biol Psychiatry.,* vol. 64, pp. 820-822, 2008.

[68] J. Ottoy, L. De Picker, J. Verhaeghe, S. Deleye, L. Wyffels, and L. Kosten, "(18)F-PBR111 PET imaging in healthy controls and schizophrenia: test-retest reproducibility and quantification of neuroinflammation. J Nucl Med. 2018;59:1267–74.," *J Nucl Med.,* vol. 59, pp. 1267-1274, 2018.

[69] G. Juckel, M. P. Manitz, M. Brune, A. Friebe, M. T. Heneka, and R. J. Wolf, "icroglial activation in a neuroinflammational animal model of schizophrenia−a pilot study," *Schizophr Res.,* vol. 131, pp. 96-100, 2011.

[70] H. W. Shelton, S. P. Gabbita, W. D. Gill, K. C. Burgess, W. S. Whicker, and R. W. Brown, "he effects of a novel inhibitor of tumor necrosis factor (TNF) alpha on prepulse inhibition and microglial activation in two distinct rodent models of schizophrenia.," *Behav Brain Res,* vol. 406, p. 113229, 2021.

[71] L. Wang *et al.*, "Targeted delivery of miR-99b reprograms tumor-associated macrophage phenotype leading to tumor regression.," *J Immunother Cancer,* vol. 8, no. 2, p.:e000517, 2020.

[72] Y. Singh *et al.*, "Mycobacterium tuberculosis controls microRNA-99b (miR-99b) expression in infected murine dendritic cells to modulate host immunity.," *J Biol Chem.,* vol. 288, no. 7, pp. 5056-5061, 2013.

[73] S. Momtazmanesh, A. Zare-Shahabadi, and N. Rezaei, "Cytokine Alterations in Schizophrenia: An Updated Review," *Front Psychiatry.,* vol. 10, no. 892, p. doi: 10.3389/, 2019.

[74] A. Vilalta and G. C. Brown, "Neurophagy, the phagocytosis of live neurons and synapses by glia, contributes to brain development and disease.," *FEBS J.,* vol. 285, no. 19, pp. 3566-3575, 2018.

[75] D. Inta, U. E. Lang, S. Borgwardt, A. Meyer-Lindenberg, and P. Gass, "Microglia Activation and Schizophrenia: Lessons From the Effects of Minocycline on Postnatal Neurogenesis, Neuronal Survival and Synaptic Pruning.," *Schizophr Bull.,* vol. 43, no. 3, pp. 493-496, 2017.

[76] M. Germann, S. G. Brederoo, and I. E. C. Sommer, "Abnormal synaptic pruning during adolescence underlying the development of psychotic disorders.," *Curr Opin Psychiatry,* vol. 34, no. 3, pp. 222-227, 2021.

[77] A. Takaoka *et al.*, "DAI (DLM-1/ZBP1) is a cytosolic DNA sensor and an activator of innate immune response.," *Nature,* vol. 448, no. 7152, pp. 501-505, 2007.

[78] T. Kuriakose *et al.*, "ZBP1/DAI is an innate sensor of influenza virus triggering the NLRP3 inflammasome and programmed cell death pathways.," *Sci Immunol.,* vol. 1, no. 2, p. aag2045, 2016.

[79] S. Hong *et al.*, "omplement and microglia mediate early synapse loss in Alzheimer mouse models.," *Science,* vol. 352, no. 6286, pp. 712-716, 2016.

[80] M. T. Heneka *et al.*, "NLRP3 is activated in Alzheimer's disease and contributes to pathology in APP/PS1 mice," *Nature,* vol. 493, no. 7434, pp. 674-678, 2013.

[81] X. Ye *et al.*, "MicroRNAs 99b-5p/100-5p Regulated by Endoplasmic Reticulum Stress are Involved in Abeta-Induced Pathologies.," *Front Aging Neurosci.,* vol. 18, no. 7, p. 210, 2015.

[82] A. D. Hart, A. Wyttenbach, V. H. Perry, and J. L. Teeling, "Age related changes in microglial phenotype vary between CNS regions: grey versus white matter differences.," *Brain Behav Immun.,* vol. 26, no. 5, pp. 754-765, 2012.

[83] P. Ayata *et al.*, "pigenetic regulation of brain region-specific microglia clearance activity.," *Nat Neurosci.,* vol. 21, no. 8, pp. 1049-1060, 2018.

[84] M. Mustapic *et al.*, "Plasma Extracellular Vesicles Enriched for Neuronal Origin: A Potential Window into Brain Pathologic Processes.," *Front Neurosci.,* vol. 11, no. 278, p. doi: 10.3389/fnins.2017.00278., 2017.

[85] A. Kumar *et al.*, "Brain cell-derived exosomes in plasma serve as neurodegeneration biomarkers in male cynomolgus monkeys self-administrating oxycodone," *EBioMedicine,* vol. 63, p. 103192, 2021.

[86] P. Langfelder and S. Horvath, "WGCNA: an R package for weighted correlation network analysis.," *BMC Bioinformatics.,* vol. 29, no. 559, p. eCollection, 2008.

[87] P. Shannon *et al.*, "Cytoscape: a software environment for integrated models of biomolecular interaction networks," (in eng), *Genome Research,* vol. 13, no. 11, pp. 2498-2504, 2003/11// 2003, doi: 10.1101/gr.1239303.

[88] G. Bindea *et al.*, "ClueGO: a Cytoscape plug-in to decipher functionally grouped gene ontology and pathway annotation networks," *Bioinformatics,* vol. 25, no. 1, pp. 1091-1093, 2009.

[89] A. T. McKenzie *et al.*, "Brain Cell Type Specific Gene Expression and Co-expression Network Architectures," *Scientific reports,* vol. 8, no. 1, p. 8868, 2018.

[90] C. Ortutay and M. Vihinen, "Immunome: A reference set of genes and proteins for systems biology of the human immune system.," *Cellular Immunology,* vol. 244, no. 2, pp. 87-89, 2006.

[91] A. R. Abbas *et al.*, "Immune response in silico (IRIS): immune-specific genes identified from a compendium of microarray expression data.," *Genes and immunity,* vol. 6, no. 4, pp. 319-331, 2005.

[92] M. R. Islam *et al.*, "A microRNA signature that correlates with cognition and is a target against cognitive decline," (in eng), *EMBO molecular medicine,* vol. 13, no. 11, p. e13659, 2021/11/08/ 2021, doi: 10.15252/emmm.202013659.

[93] C. B. Pantazis *et al.*, "A reference human induced pluripotent stem cell line for large-scale collaborative studies.," *Cell stem cell,* vol. 29, no. 12, pp. 1685-1702, 2022.

[94] W. Haenseler *et al.*, "A Highly Efficient Human Pluripotent Stem Cell Microglia Model Displays a Neuronal-Co-culture-Specific Expression Profile and Inflammatory Response.," *Stem cell reports,* vol. 8, no. 6, pp. 1727-1742, 2017.

[95] M. Goldberg *et al.*, "Exercise as a model to identify microRNAs linked to human cognition: A role for microRNA-409 and microRNA-501," *Translational Psychiatry,* vol. 11, no. 1, p. 514, 2021.

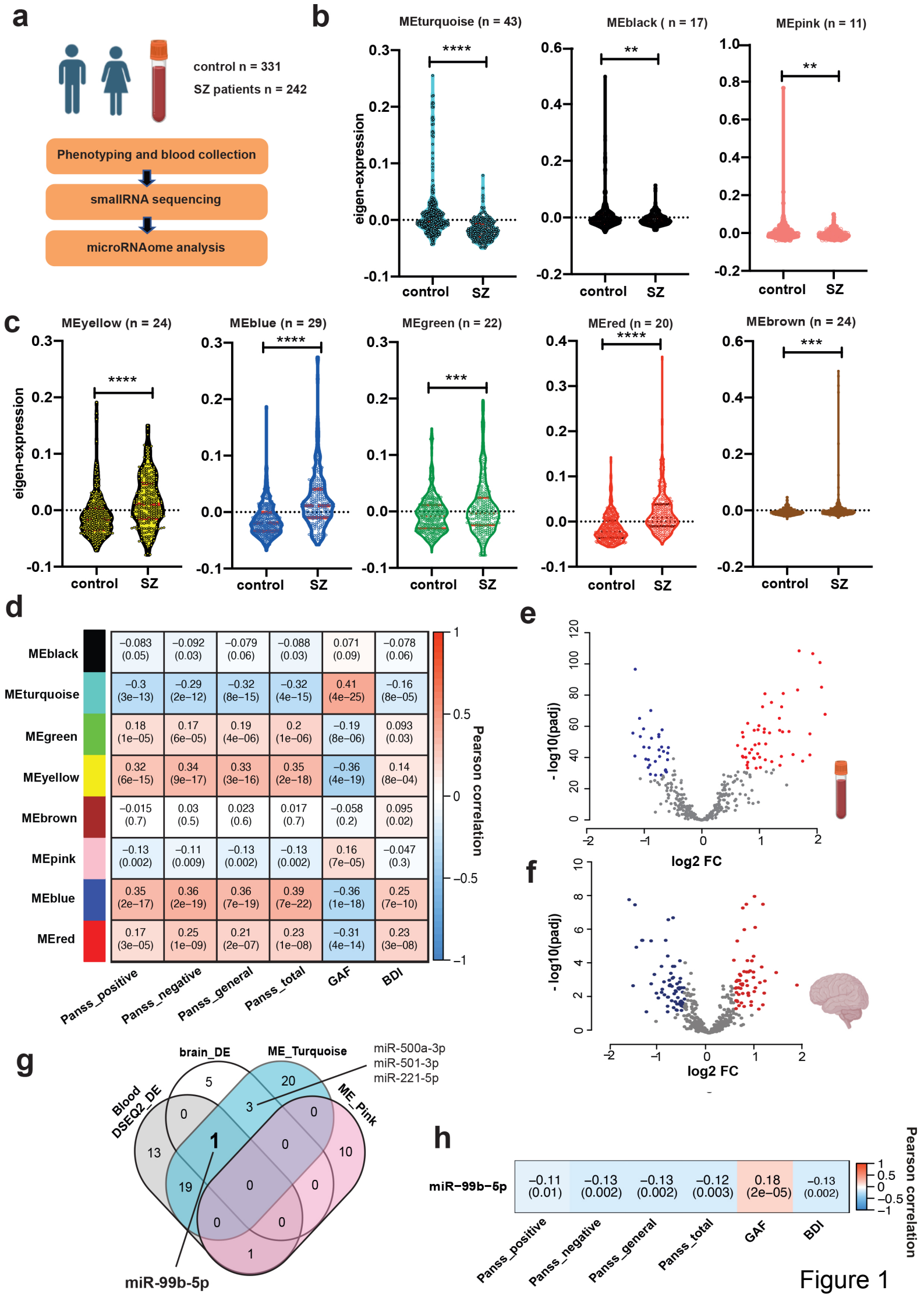
a
control n = 331
SZ patients n = 242
Phenotyping and blood collection
smallRNA sequencing
microRNAome analysis
b
MEturquoise (n = 43)
MEblack (n = 17)
MEpink (n = 11)
eigen-expression
control
SZ
c
MEyellow (n = 24)
MEblue (n = 29)
MEgreen (n = 22)
MEred (n = 20)
MEbrown (n = 24)
d
MEblack
MEturquoise
MEgreen
MEyellow
MEbrown
MEpink
MEblue
MEred
Panss_positive
Panss_negative
Panss_general
Panss_total
GAF
BDI
Pearson correlation
e
- log10(padj)
log2 FC
f
- log10(padj)
log2 FC
g
brain_DE
ME_Turquoise
Blood DSEQ2_DE
ME_Pink
miR-500a-3p
miR-501-3p
miR-221-5p
miR-99b-5p
h
miR−99b−5p
Panss_positive
Panss_negative
Panss_general
Panss_total
GAF
BDI
Pearson correlation

Figure 1

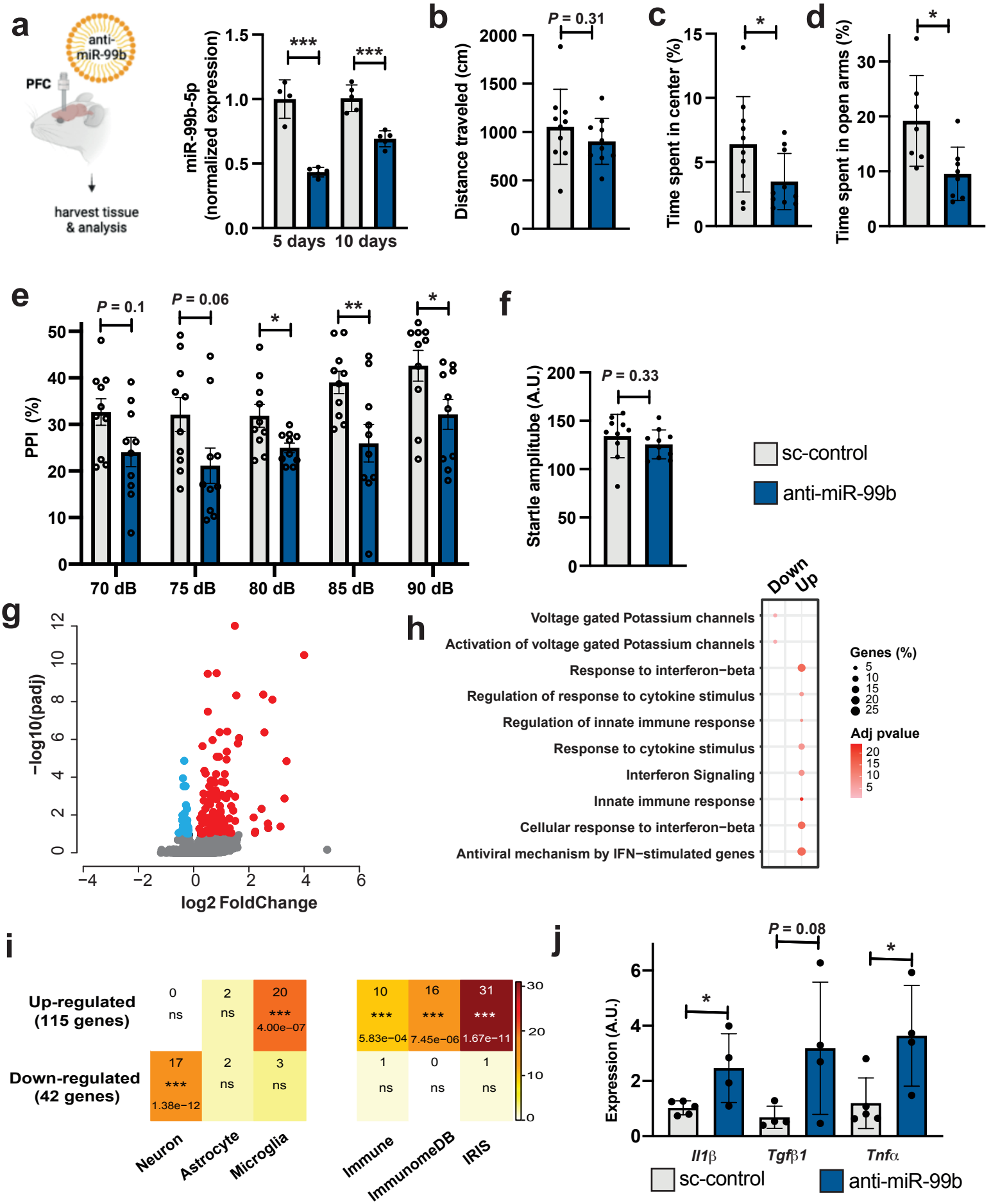
a
anti-miR-99b
PFC
harvest tissue & analysis
miR-99b-5p (normalized expression)
1.5
1.0
0.5
0.0
***
***
5 days
10 days
b
P = 0.31
Distance traveled (cm)
2000
1500
1000
500
0
c
*
Time spent in center (%)
15
10
5
0
d
*
Time spent in open arms (%)
30
20
10
0
e
P = 0.1
P = 0.06
*
**
*
PPI (%)
50
40
30
20
10
0
70 dB
75 dB
80 dB
85 dB
90 dB
f
P = 0.33
Startle amplitude (A.U.)
200
150
100
50
0
sc-control
anti-miR-99b
g
−log10(padj)
12
10
8
6
4
2
0
−4
−2
0
2
4
6
log2 FoldChange
h
Down
Up
Voltage gated Potassium channels
Activation of voltage gated Potassium channels
Response to interferon−beta
Regulation of response to cytokine stimulus
Regulation of innate immune response
Response to cytokine stimulus
Interferon Signaling
Innate immune response
Cellular response to interferon−beta
Antiviral mechanism by IFN−stimulated genes
Genes (%)
5
10
15
20
25
Adj pvalue
20
15
10
5
i
Up-regulated (115 genes)
Down-regulated (42 genes)
0
ns
2
ns
20
***
4.00e−07
17
***
1.38e−12
2
ns
3
ns
10
***
5.83e−04
16
***
7.45e−06
31
***
1.67e−11
1
ns
0
ns
1
ns
30
20
10
0
Neuron
Astrocyte
Microglia
Immune
ImmunomeDB
IRIS
j
P = 0.08
*
*
Expression (A.U.)
6
4
2
0
Il1β
Tgfβ1
Tnfα
sc-control
anti-miR-99b

Figure 2

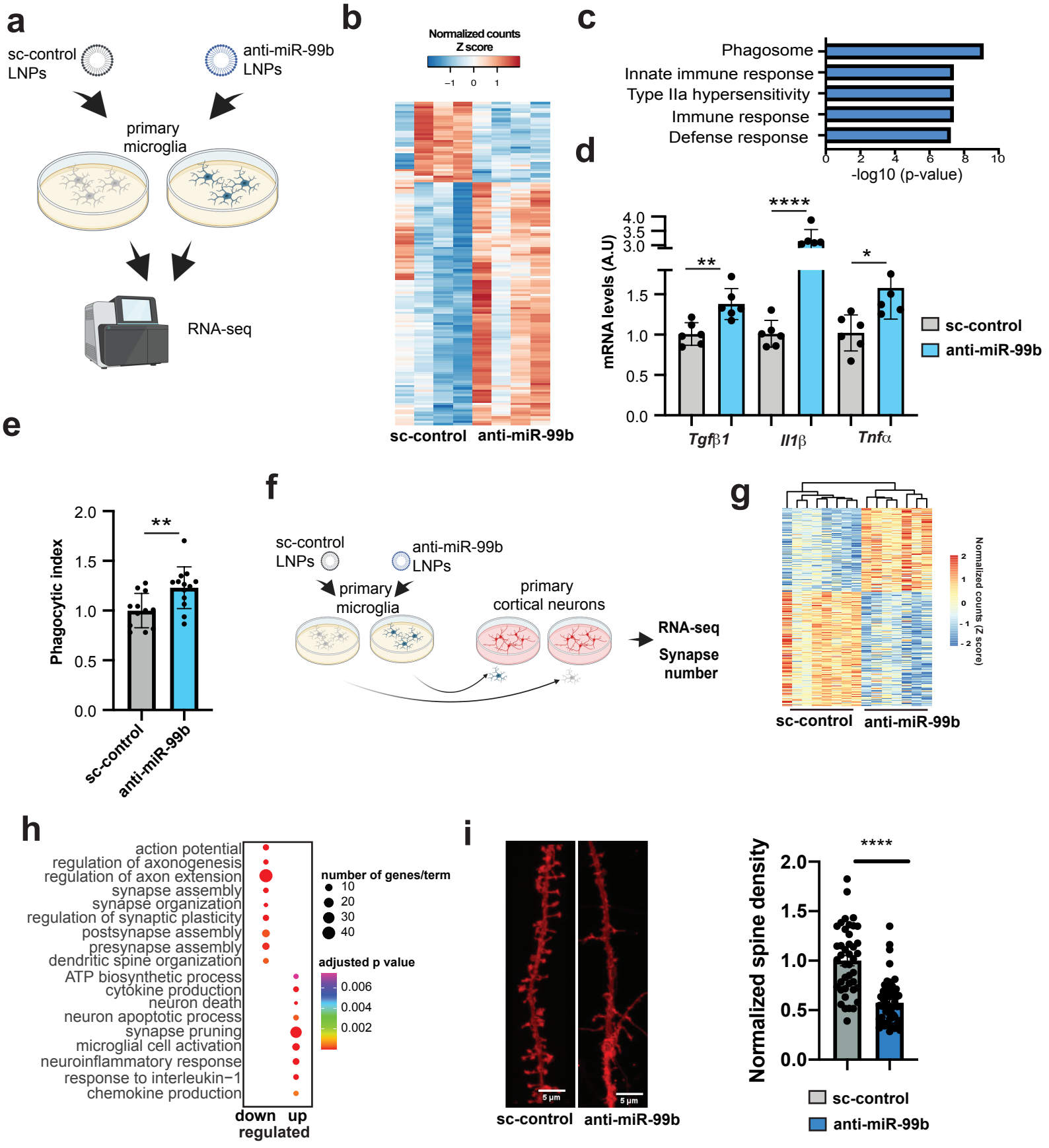
a
sc-control LNPs
anti-miR-99b LNPs
primary microglia
RNA-seq
b
Normalized counts Z score
−1 0 1
sc-control
anti-miR-99b
c
Phagosome
Innate immune response
Type IIa hypersensitivity
Immune response
Defense response
0 2 4 6 8 10
-log10 (p-value)
d
mRNA levels (A.U)
4.0 3.5 3.0 1.5 1.0 0.5 0.0
**
****
*
Tgfβ1
Il1β
Tnfα
sc-control
anti-miR-99b
e
Phagocytic index
2.0 1.5 1.0 0.5 0.0
**
sc-control
anti-miR-99b
f
sc-control LNPs
anti-miR-99b LNPs
primary microglia
primary cortical neurons
RNA-seq
Synapse number
g
Normalized counts (Z score)
2 1 0 -1 -2
sc-control
anti-miR-99b
h
action potential
regulation of axonogenesis
regulation of axon extension
synapse assembly
synapse organization
regulation of synaptic plasticity
postsynapse assembly
presynapse assembly
dendritic spine organization
ATP biosynthetic process
cytokine production
neuron death
neuron apoptotic process
synapse pruning
microglial cell activation
neuroinflammatory response
response to interleukin−1
chemokine production
down regulated
up regulated
number of genes/term
10 20 30 40
adjusted p value
0.006 0.004 0.002
i
5 µm
5 µm
sc-control
anti-miR-99b
Normalized spine density
2.0 1.5 1.0 0.5 0.0
****
sc-control
anti-miR-99b

Figure 3

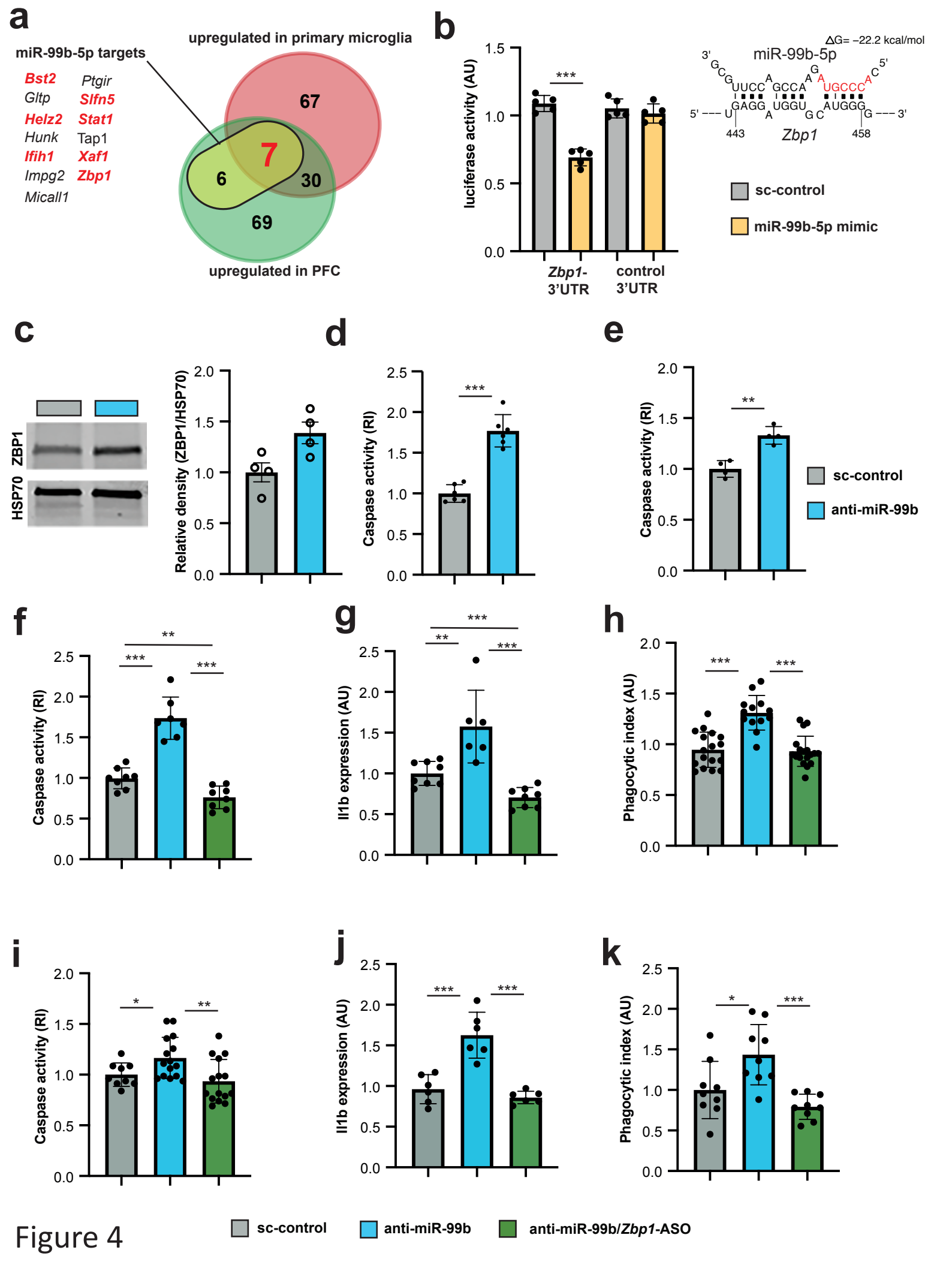
a
miR-99b-5p targets
Bst2
Ptgir
Gltp
Slfn5
Helz2
Stat1
Hunk
Tap1
Ifih1
Xaf1
Impg2
Zbp1
Micall1
upregulated in primary microglia
upregulated in PFC
67
7
6
30
69
b
luciferase activity (AU)
***
Zbp1-3'UTR
control 3'UTR
ΔG= −22.2 kcal/mol
miR-99b-5p
Zbp1
443
458
sc-control
miR-99b-5p mimic
c
ZBP1
HSP70
Relative density (ZBP1/HSP70)
d
Caspase activity (RI)
e
anti-miR-99b
f
g
Il1b expression (AU)
h
Phagocytic index (AU)
i
j
k
sc-control
anti-miR-99b
anti-miR-99b/Zbp1-ASO

Figure 4